THE GENERATION OF AN EXPERIMENTAL DATABASE FOR TESTING PREDICTIVE MODELS FOR α-PINENE GAS- AND PARTICLE-PHASE REACTIONS IN THE ATMOSPHERE

Jyoti Bapat

A thesis submitted to the faculty of the University of North Carolina at Chapel Hill in partial fulfillment of the requirements for the degree of Master of Science in the Department of Environmental Sciences and Engineering, Gillings School of Global Public Health.

Chapel Hill
2011

Approved by

Professor Richard M. Kamens, Advisor

Assistant Professor William G. Vizuete, Reader

Assistant Professor Jason D. Surratt, Reader

ABSTRACT

Jyoti Bapat

The Generation of an Experimental Database for Testing Predictive Models for α-Pinene Gas- and Particle-Phase Reactions in the Atmosphere

(Under the direction of Professor Richard M. Kamens)

Atmospheric chemistry of biogenic and anthropogenic volatile organic compounds (VOCs) has become an increasingly important aspect of environmental policy. Atmospheric oxidation of VOCs produces ozone (O_3) and particulate matter (PM), both of which have been shown to have effects on climate and human health. α-Pinene, a biogenically emitted VOC, is a source of O_3, and in an urban environment is an important source of urban secondary organic aerosol (SOA). This work attempts to model the O_3 and SOA production of α-pinene photooxidation in the presence of oxides of nitrogen (NO_x) and an urban hydrocarbon (HC) mixture. The model was compared against recent experimental data. Under most conditions, the model predicts SOA production well, and fits gas-phase data better than other common mechanisms. Results indicate that further experimentation is required to model α-pinene chemistry at α-pinene/NO_x ratios lower than 1, especially since these are concentrations that are atmospherically relevant.

ACKNOWLEDGEMENTS

I owe my deepest gratitude to my parents, Ashok and Mina Bapat, and my brother, Deepak Bapat, for their love and support. They have encouraged every one of my endeavors and for that I am truly grateful.

This thesis would not have been possible if it were not for Professor Rich Kamens, who not only served as my advisor, but challenged and encouraged me from the day that I joined his group. I would also like to thank the members of my committee, Dr. Will Vizuete and Dr. Jason Surratt, for their advice and guidance.

Special thanks go to Haofei Zhang and Harshal Parikh, who have been invaluable resources and colleagues throughout my time at UNC.

Lastly, I would like to thank the friends I've made along the way, from my youth and time at Carnegie Mellon to my lab and classmates at UNC, for their support, encouragement, and friendship over the past two years without which the writing of this thesis would not have been possible.

TABLE OF CONTENTS

LIST OF TABLES

Table

LIST OF FIGURES

Figure

Chapter I

INTRODUCTION

α-Pinene (2,6,6-trimethyl-bicyclo[3.1.1]hept-2-ene) is an important biogenic volatile organic compound (VOC) in the class of monoterpenes, all of which have the chemical formula $C_{10}H_{16}$. α-Pinene is naturally emitted through the oil of a number of coniferous and non-coniferous plants, most notably from pine trees (Blanch, et al., 2011). It has been demonstrated that atmospheric oxidation of α-pinene creates ozone (O_3) and forms a number of low saturation vapor-pressure products which can condense onto pre-existing particles or create new aerosols via nucleation; therefore, α-pinene is an important contributor to global secondary organic aerosol (SOA) production (Guenther et al., 1995). α-Pinene oxidation also causes O_3 production near the Earth's surface, which has been shown to have adverse health effects on humans (Hackney et al., 1975; Krupnick et al., 1990). SOA have also been demonstrated to have potential health effects (Pope et al., 2002). Additionally, SOA have direct effects on climate by reflecting sunlight back to space, cooling the Earth (Solomon, et al., 2007; Hallquist et al., 2009). For these reasons, both O_3 and SOA have become important in atmospheric science and policy.

It is estimated that the total global emissions of α-pinene are around 127 TgC/year, which is approximately 11% of total biogenic VOC emissions (Guenther et al., 1995). α-Pinene photochemistry is complex, creating products in both gas- and particle-phase systems, and exhibits dependencies on both temperature and relative humidity (Tillmann et al., 2010;

Zhang et al., 2010). The gas-phase products of α-pinene are well documented (Yu et al., 1998; Jang et al., 1999). A few significant gas-phase products of α-pinene are pinonaldehyde and norpinonaldeyhde, pinic and norpinic acid, pinonic and norpinonic acid, among others. Identification of some of the particle-phase products has also been previously described (Kamens et al., 1999; 2001). Estimations of SOA production range from 2 to 79 Tg/year (Kanakidou et al., 2000; Tsigaridis et al., 2003).

Attempts have been made to model α-pinene oxidation. The Carbon Bond mechanisms, CB4 (Gery et al., 1989) and CB05 (Yarwood et al., 2005) use an engineered method to represent atmospheric chemistry, with chemical species based on functional groups and reactivity. SAPRC07 (Carter et al., 2009) is an example of a lumped mechanism, and represents chemistry a little more explicitly than the Carbon Bond mechanisms. The Master Chemical Mechanism version 3.1(MCMv3.1) is a semi-explicit mechanism, and details a number of oxidation reactions for α-pinene (Jenkin et al., 1997; Saunders et al., 2003). Limitations exist with both of these mechanistic methods. Lumped or engineered mechanisms, like SAPRC and the Carbon Bond mechanisms, are too condensed to represent many types of gas-phase products and SOA precursors. On the other hand, explicit mechanisms contain a large number of reactions, and are therefore too big to use in current air quality models. For this reason, a mechanism with fewer reactions than MCMv3.1, but more specific than either Carbon Bond or SAPRC, is needed.

UNC's version of the α-pinene photo-oxidation mechanism (Kamens et al., 2001) is more explicit than CB05 and SAPRC07, and still much more condensed than MCMv3.1. The original mechanism was written in 2001 and used a solver called Photochemical Kinetics Simulation System (PKSS) (Jeffries, 1991; Kamens et al., 1999; Kamens et al., 2001). In

1998, Jeffries developed a more sophisticated kinetic solver, called Morphocule (MORPHO), which could accommodate a far greater number or species and reactions, and is only limited by the size or memory on the computer.

Besides accommodating for a large number of species, MORPHO also allows the user at each time step to sum related species into a scalar quantity, and permits the sum of these individual species to react with other individual species. This is particularly useful for the representation of peroxy radical (RO_2) cross reactions, and also permits all particle-phase products to be grouped together, and then react with individual gas phase-species, simulating gas-phase condensation to the particle phase. Another feature of MORPHO is that it allows the several individual mechanisms to be run in tandem. For example, two mechanisms written separately for two VOCs and saved as separate files can be run in conjunction to simulate the photooxidation of those VOCs in the presence of each other. These features make MORPHO a much more flexible solver to use with these mechanisms.

A number of recent studies have discovered new gas- and particle-phase products that call for an update on the original α-pinene photo-oxidation mechanism (Claeys et al., 2009; Szmigielski et al., 2007; Yasmeen, et al., 2010). In addition, there have been several updates on major reaction rates (Jenkin et al, 1997; Saunders et al., 2003). The goal of this work was to update the existing gas- and particle-phase mechanisms for α-pinene atmospheric reactions that had been written at UNC (Kamens et al., 2001) and evaluate this mechanism with a more complete α–pinene database generated in the UNC outdoor smog chamber facility over the summer of 2009, 2010, and 2011. Previous experiments at UNC generally have initial conditions that are very high, reaching 1 ppmV, and there is a need to extend experimental databases to concentrations of 0.1 ppmV and lower.

Although α-pinene contributes considerably to global terpene emissions (Guenther et al., 1993; 1995), on an urban scale it can contribute substantially to urban SOA formation (Lewandowski et al., 2008). Hence, there is a need not only for α-pinene – NO_x experiments, but experiments in which α-pinene reacts within the atmospheric environment of an urban hydrocarbon mixture. In addition, since other compound classes such as aromatics also generate SOA, there is a need to test SOA simulation models that contain α-pinene in the presence of aromatics. Both of these conditions are investigated in this work. A combination of the two, α-pinene photo-oxidation in the presence of both aromatics and an urban hydrocarbon mixture, is also considered.

Chapter II

EXPERIMENTAL

Chamber Description

A series of experiments were performed in UNC's Ambient Air Research Facility dual outdoor smog chamber located in Pittsboro, North Carolina, over the summers of 2009, 2010, and 2011. The smog chamber is made out of clear FEP Teflon, and a sheet of the same material separates the chamber into two sides. One side, called "North", is 136 m^3. The other side, called "South", has a volume of 138 m^3. The dual chambers allow two simultaneous experiments with different concentrations and species of VOCs to be run at the same time under the same meteorological conditions. The chamber sits above a sampling laboratory. Gas- and particle-phase sampling lines run from both sides of the chamber through the floor into the room below, which houses all instrumentation as well as the air compressor. All experiments were performed under clear skies with natural sunlight, at ambient relative humidity (RH), and at ambient temperatures ranging from 285 to 315 K. An image of the chamber can be seen below in Figure 1.

Figure 1. UNC dual chamber located in Pittsboro, North Carolina

Methods

For at least six hours prior to each experiment, the chambers were purged with rural North Carolina air. Sulfur hexafluoride (SF_6) was injected into each side of the chamber to track dilution through the chamber walls. Different amounts of nitrogen oxides (NO_x = NO + NO_2) were then injected into the chamber from a high-pressure gas cylinder. The injection of NO_x occurred before the addition of any hydrocarbons, to titrate out any ambient O_3 in the chamber. Concentrations of NO_x, O_3, and VOCs were monitored by on-site instrumentation housed in the sampling laboratory under the chamber.

To simulate an urban air mixture, a gas mixture of eleven hydrocarbons of varying concentrations, called the UNC hydrocarbon gas mixture (HCMix), was injected into the chamber prior to the addition of the VOC. The composition of hydrocarbons in HCMix is shown in Table 1. α-Pinene or toluene was then injected into the chamber by vaporizing the pure liquid in a U-tube and flushing the hydrocarbon into the chamber with a flow of pure N_2 gas. After each injection, a series of mixing fans were turned on. These served a dual purpose in that they flushed out the gas lines going into the chamber as well as mixed the air in the chamber, ensured a well-mixed reactor.

Table 1. HCMix composition

Compound	**Concentration (ppmC)**
isopentane	0.16135
n-Pentane	0.25285
2-methylpentane	0.08363
2,4-dimethylpentane	0.08301
2,2,4-trimethylpentane	0.11157
1-butene	0.02805
cis-2-butene	0.03074
2-methylbutene	0.02753
2-methyl-2-butene	0.03923
ethylene	0.13051
propylene	0.05154
Total	**1.00001**

Each experiment was run for approximately twelve hours. Gas-phase species (NO, NO_2, O_3) were measured every minute, particles were counted and measured for size approximately every five minutes, and temperature was measured every thirty minutes. Gas-phase organic species were monitored throughout the experiment with the use of gas chromatography (GC).

Filter samples of SOA were taken during the experiment on October 18th, 2010. One borosilicate microfiber filter (PALL Life Sciences, 47-mm diameter, 1.0-μm pore size) on each side of the chamber was pulled for an hour before the injection of any hydrocarbons to get a reading on background aerosol. After the injection of hydrocarbons, another set of filters was set up on both sides of the chamber, pulling aerosol for approximately two hours. A third and final set of filters was used to pull aerosol from the chamber for an additional two hours. The flow rate for each filter-sampling period was approximately 25 L/min. Each set of filters was actually two filters, a filter on top which was separated by a 4 mm filter holder from the filter on the bottom. The top filter would collect aerosols, and the bottom filter would collect only gaseous organics that were absorbed onto each filter (McDow et al., 1990). To get the mass of just the aerosols deposited on the top filter within the two hours, the mass of the bottom filter, or the gas-phase product deposition, was subtracted from the top filter.

The filters were extracted using 8 mL high purity methanol (LC-MS CHROMASOLV-grade, from Sigma-Aldrich) through 45 minutes of sonication. The extracted product in methanol was blown dry under a gentle stream of N_2. The dry product was dissolved in 150 μl acetonitrile (HPLC grade, from Fisher Scientific), and was then analyzed using gas chromatography interfaced to quadrupole mass spectrometry (GC/MS).

The GC/MS instrument was equipped with an electron ionization (EI) source that was operated at 70 eV (Hewlett 5890 Packard Series II Gas Chromatograph interfaced to a HP 5971A Series Mass Selective Detector, Econo-Cap-EC-5 column, 30 m×0.25 mm×0.25 μm). The GC/MS method was run on SCAN mode with a solvent delay of 3 minutes. An initial inlet temperature of 250°C and pressure of 3 psi was used. Initial oven temperature was 80°C and final oven temperature was 250°C. Total run time for the method was 22 minutes. Blank filters spiked with a pinonic acid standard (Sigma-Aldrich, 98%) were also run through the same extraction procedure, to determine extraction efficiency and the degree of retention through the drying process. All samples included two internal standards: bornyl acetate and methyl dodecanoate. These two internal standards were chosen because their volatilities fell within the range of volatilities of known α–pinene products. Known amounts of both internal standards were injected into each filter sample and standard. All samples were analyzed using GC/MS within 30 hours of being extracted and concentrated.

Instrumentation

During each experiment, NO_x and O_3 mixing ratios were monitored using a chemilumicescent NO_x meter (9841A Teledyne Instruments Monitor Labs, Englewood, CO) and an ultraviolet O_3 meter (49 Thermo Electron Instruments, Hopkinton, MA). Both of these meters were calibrated before each experiment using a NIST certified NO_x tank. The outdoor chamber facility is also equipped with two scanning mobility particle sizers (SMPS), which are both composed of a differential mobility analyzer (DMA) (TSI Long DMA, 3081, MN, USA) interfaced with a condensation particle counter (CPC) (TSI CPC, 3025A, MN, USA), that are used for particle counting and sizing. Gas-phase organic species were tracked using a

GC (Shimadzu Model 14A, column: 30 m, 0.25mm i.d., J&W DB-1, 0.25m film thickness) coupled to a flame ionization detector (FID). The method was run for ten minutes at an oven temperature of 50°C and held isothermally through the entire run. Every GC was calibrated before each experiment using a mix of eight basic hydrocarbons ranging in number of carbons. The lab also includes instrumentation for measuring SF_6 and peroxyacetyl nitrate (PAN). RH was measured using a RH Analyzer (Sable Systems RH-100, Las Vegas, NV, USA). Solar irradiance in the chamber was measured using a Black and White Pyranometer (Eppley Laboratories, Model 8-48, RI).

Chapter III

MECHANISM DEVELOPMENT

Original Gas-Phase Mechanism Development

The basis of the α-pinene photolysis mechanism is the 2001 version written by Kamens et al., (1999; 2001). A list of compounds and their abbreviations used in the mechanism is given in Appendix B Table B-1 and B-2 at the end of this manuscript. The main reaction pathway for α-pinene oxidation in the atmosphere is through hydroxyl radical (OH) attack (Kamens et al., 1999). Through OH addition to the double bond, two similar peroxy (RO_2) radicals are generated, and these were grouped together in the mechanism as 'ap-oo'. This RO_2 radical undergoes further reaction with nitric oxide (NO) to ultimately produce pinonaldehyde and organic nitrates, along with nitrogen dioxide (NO_2) and hydroperoxyl radicals (HO_2). Attack by the NO_3 radical on the α-pinene double bond is also possible, resulting in organic nitrates (Atkinson, 1990; 1997). α-Pinene reaction with O_3 is also depicted, resulting in the production of two Criegee bi-radicals which undergo further reaction to produce a number of RO_2 radicals and stable products. Two of the most important gas-phase products of α-pinene chemistry, pinic and pinonic acid, are formed from the O_3 and OH pathways (Kamens et al., 2001).

This original mechanism (Kamens et al., 2001) includes photolysis reactions of pinonaldehyde, oxypinonaldehyde, pinalic acid, and two RO_2 radicals. Each photolysis rate

coefficient, J, was calculated using Equation 1. Light flux, Γ, is based on measurements from one of the UNC outdoor smog chambers (Jeffries et al., 1989). The cross section (σ) and quantum yield (Φ) are both dependent upon the species being photolyzed, and are based upon the International Union of Pure and Applied Chemistry (IUPAC, 2002) and Jet Propulsion Laboratory (JPL) (Sander et al., 2006) suggested values.

$$J_i = \int_{\lambda_1}^{\lambda_2} \Gamma^{\Theta}(\lambda)\sigma_i(\lambda)\Phi_i(\lambda)\, d\lambda \quad (1)$$

Most recently, this mechanism was updated in 2007 (Li et al., 2007) with the addition of oligomerization reactions. These are represented by a series of reactions in which particle-phase products combine to form an oligomer, called "seed1" in this mechanism. Throughout the discussion, this version of the mechanism will be referred to as the 2001 mechanism, including gas- and particle-phase chemistry and oligomerization. Reaction rates and yields from this mechanism come from previous works (Kamens et al., 2001; Li et al. 2007)

Original Particle-Phase Mechanism Development

Eventually, the organics produced from α-pinene photo-oxidation undergo a series of oxidation steps, the products of which have low vapor pressures allowing them to condense onto available particles. These are represented in the mechanism as 9 different particle-phase species. The particle-phase species and their corresponding gas-phase species are defined in the Appendix B.

Rate constants for partitioning to and from the particle-phase were calculated originally by Kamens, et al. (1999, 2001). The partitioning coefficient, K_p, is equal to the ratio of the rates of the forward and backward reactions, k_{on} and k_{off}, respectively (Equation 2). K_p was calculated using an absorptive portioning model, a condensed form of which is

shown below in Equation 3. Vapor pressure, p_L, can be calculated using Equation 5. Entropy of vaporization, ΔS_{vap}, can be calculated using the boiling point of each species, which was estimated using empirical methods based on chemical structure determined by Joback, et al. (1987). The Joback calculation of boiling points uses a combinatorial method to estimate the contribution of specific groups. The reaction rate for partitioning from the particle to the gas phase is k_{off} (Equation 4). In this equation, E_a is the activation energy required for the absorption to take place. This activation energy can be calculated by assuming a roughly linear relationship between activation energy and the natural log of vapor pressure of the compound. The pre-exponential factor, β, is equal to $k_b/h*T$, where k_b is Boltzmann's constant, h is Planck's constant, and T is the ambient temperature. Since k_b and h are constant, and temperature does not change significantly over the course of a day, an average of temperature of 298K was used to calculate β. The method of partitioning rate calculations has been described in previous works (Kamens et al., 1999).

$$K_p = k_{on}/k_{off} \tag{2}$$

$$K_p = \frac{7.501 \times RT}{10^9 \times MW_{om}{}^{i} \times p_L{}^{o}} \tag{3}$$

$$k_{off} = \beta \times e^{\left(-\frac{Ea}{RT}\right)} \tag{4}$$

$$\ln(p_L) = \frac{\Delta S_{vap} T_b}{R}\left[1.8\left(1 - \frac{T_b}{T}\right) + 0.8(\ln\frac{T_b}{T})\right] \tag{5}$$

The original mechanism also accounted for the loss of both gas and particle products to the walls. The wall-loss of gas-phase species was estimated from observed pyrene loss to the walls at 271K and 297K (Kamens et al., 1999). The loss of particle-phase species to the walls was estimated using a similar method, adjusting for dilution (Kamens et al., 1999).

α-Pinene Mechanism Modifications

The α-pinene mechanism was last updated in 2007, with the addition of only a few reactions detailing the formation of oligomers from particle-phase reactions (Li et al., 2007). Since that time, several new developments in the atmospheric chemistry of α-pinene have been published (Claeys et al., 2009; Szmigielski et al., 2010; Yasmeen et al., 2010). There have also been updates in rate constants. Rate constant changes have been determined through either further research or a change in the accepted atmospheric rate constant suggested by the International Union of Pure and Applied Chemistry (IUPAC). The complete mechanism is given in Appendix B, and major mechanism updates from rate constants are given in this section in Tables 2 and 3.

The production of high-molecular weight species from α-pinene oxidation has been documented in a few recent studies through the use of liquid chromatography interfaced to mass spectroscopy (LC/MS). This includes compounds such as terpenylic acid, 2-hydroxyterpenylic acid, and diaterpenylic acid acetate (Claeys et al., 2009; Yasmeen et al., 2010), which have molecular weights of 172, 188, and 232, respectively. In addition, LC/MS has been used to detect oligomeric species from smog chamber studies of α-pinene oxidation (Gao et al., 2004; Tolocka et al., 2004; Hall et al., 2010) as well as organosulfate formation in α-pinene SOA generated in the presence of NO_x and acidified sulfate seed aerosol (Surratt et al., 2007; 2008). Analysis of α-pinene SOA using LC/MS has provided tentative structures; however, formation mechanisms and yields of these compounds have not been fully elucidated, due to the fact that authentic standards have been lacking. For that reason, they were not included in the updated mechanism. These compounds, however, may be of significance because of their high molecular weights. This means they have lower volatilities

than other significant α-pinene oxidation products, and therefore will have a potentially greater contribution to SOA production.

Recently, a high-molecular weight compound with three carboxylic acid groups was identified as a product of α-pinene oxidation with the OH radical (Szmigielski et al., 2010). 3-methyl-1,2,3-butane-tricarboxylic acid (MBTCA), an eight carbon carboxylic acid with a molecular weight of 204, is formed in several stages from the reaction of pinonic acid with the OH radical. A mechanism for formation has been proposed by Szmigielski et al. (2010), who suggest that MBTCA may form directly in the particle phase. This proposed reaction sequence was condensed to two reactions for inclusion in this mechanism. Starting with the reaction of pinonic acid and the OH radical, this sequence results in the formation of an intermediate product, 'pre-tri', which stands for the pre-tricarboxylic acid product.

Originally, in the reaction of the α-pinene nitrate RO_2 with NO_3, there was only one stoichiometric equivalent of nitrogen generated. This reaction was modified to produce a di-nitrate product, called 'OH-apN2O6', to maintain a nitrogen mass balance. The production of an α-pinene di-nitrate product has been documented by Spittler, et al (2006). The α-pinene nitrate RO_2 radical undergoes addition of NO to form a di-nitrate product, called 'OH-apN2O6' in the mechanism (Equation 6). As Spittler et al. (2006) stated, while this may not be significant in heavily forested areas, this pathway may be more important in high-NO_x regions such as areas with heavy vehicle traffic. NO_3 chemistry also becomes more significant at night, when the lack of sunlight makes reactions with the OH radical minimal.

In the original mechanism, RO_2 radical cross reactions were limited due to limitations in the number of reactions and species allowed (Kamens et al., 2001). This meant that only the most important RO_2 cross reactions were considered. In reality, all RO_2s cross react with

each other. MORPHO allows for this to be represented quite simply. All RO_2s were combined into a scalar value called "RO_2" (Leungsakul et al., 2005). Multiplying the rate constant of a reaction by this value is the equivalent of having the reactant in each reaction react with the entire group "RO_2". This process was performed for all RO_2 cross reactions, combining a number of reactions. These equations can be seen in R[AP_54] to R[AP_61] in Appendix B.

To update rates for the α-pinene mechanism, important reactions were first compared with the Master Chemical Mechanism v3.1 (MCMv3.1). MCMv3.1 provides comprehensive experimental reaction rates for each major reaction. MCMv3.1 is the most explicit mechanism out of all widely used mechanisms. In MCMv3.1, in the case that a rate of reaction has not been experimentally determined, a generic rate is assigned. For example, MCMv3.1 has a generic rate constant for all NO + RO_2 reactions is 2.7E-12*EXP(360/T). Similarly, there are universal rate constants for RO_2 + HO_2 reactions, RO_2 + NO_3 reactions (Jenkin et al., 1997; Saunders et al., 2003).

In addition to MCMv3.1, the IUPAC Subcommittee for Gas Kinetic Data Evaluation compares all experimentally derived rate constants for the main, important reactions of VOCs and atmospheric oxidants. For α-pinene, IUPAC publishes rate constants for reactions with O_3, OH, and NO_3. IUPAC also publishes rate constant data for the main α-pinene photo-oxidation product, pinonaldehyde. The database includes rate constants for the reaction of pinonaldehyde with O_3, OH, and NO_3. Several rate constants in the 2001 α-pinene reaction were updated with their counterparts from the MCMv3.1for from the IUPAC Subcommittee for Gas Kinetic Data Evaluation recommendations. These are displayed in Tables 2 and 3 (Dlugokencky et al., 1989; Hallquist et al., 1997; Davis et al., 2007).

All of these additions were necessary to keep the mechanism up to date. However, they did not create a significant amount of additional O_3. Even with the inclusion of these mechanisms, the model was still under predicting O_3 in experiments with low concentrations of α-pinene, as shown later in the Results and Discussion section. A few changes did influence the amount of O_3 produced. These changes are outlined below.

Another change to the gas-phase α-pinene mechanism was an adjustment in the representation of acetone. Previously, acetone was represented as a dead-end product (Kamens et al., 2001). It was explicitly created, but did not react further. This original α-pinene mechanism was coupled with CB4, which did not include acetone reaction chemistry (Gery et al., 1989). However, CB05 includes atmospheric acetone chemistry, where one molecule of acetone has the same reactivity as three PAR, or three singly-bonded one-carbon atom components (Yarwood et al., 2005). All acetone molecules were converted to PAR by multiplying the stoichiometric coefficient of the acetone by three. This allows for the simulation of acetone reacting with oxidants in the atmosphere, as it would in reality. Although acetone is relatively long-lived in the atmosphere, a small amount of acetone oxidation does occur. This means that ultimately, the change of the species from one acetone to three PAR increases O_3 production, as happened in this case.

Reaction R[AP_64] was added to the mechanism to simulate the decomposition of the α-pinene organic nitrate to NO_2 and pinonaldehyde (Equation 7). This change was made to try and increase O_3 production from the model, as the photolysis of NO_2 can create O, which reacts with O_2 to create O_3. This only slightly increased the overall production of O_3. The rate for this reaction in MCMv3.1 is 5.5E-12, and is based off of the reaction of the OH radical and APINANO3 (Jenkin et al, 1997; Saunders et al., 2003). For use in the mechanism, it was

raised to 1.5E-11, to try and produce as much NO_2 as possible without affecting the production of PAN and other nitrates. This value is the upper limit of this rate constant; if raised any more, the solver was unable to compile the mechanism.

R[AP_4] = 'apNO3-oo' + NO → 0.81*NO2 + 0.19*'OH-apN2O6' + 0.81*'OH-apNO3' + 0.81*HO2 @4.10E-12*EXP(180/TK) (6)

R[AP_64] = 'OH-apNO3' + OH → NO2 + pinald @1.5E-11 (7)

Table 2. Changes to Rate Constants from MCMv3.1

Reaction	**Rate was:**	**Rate changed to:**
R[AP_19]	2.60E-13*EXP(1250/TK)	2.65E-13*EXP(1300/TK)
R[AP_27]	4.10E-12*EXP(180/TK);	7.15E-12*EXP(290/TK)
R[AP_64]	Did not exist	1.5E-11

Table 3. Changes to Rate Constants from the IUPAC: Subcommittee for Gas Kinetic Data Evaluation

Reaction	**Rate was:**	**Rate changed to:**
R[AP_3]	3.50E-13*EXP(818/TK)	1.2E-12*EXP(490/TK)
R[AP_23]	9.1E-11	3.9E-11
R[AP_26]	5.39E-14	2.0E-14

Adjustments were also made to the particle-phase portion UNC's α-pinene oxidation mechanism. Part8 and part9, two new particle-phase products, were added. Part8 is the partitioning product of 'pre-tri', the new pinonic acid oxidation product with thee carboxylic acid groups. Part9 is the partitioning product of the α-pinene di-nitrate, called 'OH-apN2O6' in this mechanism, which was produced in R[AP_4], shown in Equation 7 above.

Besides the addition of these two reactions, changes were made to the partitioning constants for all particle-phase products. This includes both k_{on}, the rate of partitioning to the particle phase, and k_{off}, which is the rate of partitioning back to the gas phase. These were calculated using the Joback method of estimating the boiling point, which was used to

calculate the vapor pressure and change in entropy of the reaction, or ΔS. Partitioning rate constants were also calculated for the two new particle-phase products.

One significant change from the original mechanism is the inclusion of temperature-dependant rate constants for partitioning to the particle phase. K_p, the ratio of partitioning onto and off of the particle phase was calculated using the molecular weight, temperature, and estimated vapor pressure of the species at that temperature, as described above. k_{off} was calculated using the temperature and estimated vapor pressure of each species as described in Equations 4 and 5. For the calculation of k_{on}, a different k_{off} was determined for each temperature and multiplied by its corresponding K_p. β is the ratio of Boltzmann's constant to Planck's constant, and is only dependant only these two constants and temperature. Since the ratio is much larger than temperature, there was not a significant difference in β over the temperature range, and an average β was used for k_{off}. In the original mechanism only k_{off} was temperature-dependent. Even from calculating k_{on} at different temperatures, it was clear that there was temperature dependence to partitioning onto the particle phase. However, there is no direct calculation to determine a temperature-dependant k_{on}. To work around this, temperature was plotted against the rate constant, and an exponential curve was fit to the plot. This exponential equation became the new temperature-dependant rate constant for k_{on}. New values for each partitioning reaction rate are shown in Table 4.

Table 4. Partitioning Constants for all Particle-Phase Species

	k_{on}	k_{off}
part	2.198E-4*EXP(-6568/TK)	6.2167E12*EXP(-10142/TK)
part1	2.66E-5*EXP(-6320/TK)	6.2167E12*EXP(-9392/TK)
part2	1.889E-6*EXP(-5030/TK)	6.2167E12*EXP(-8693/TK)
part3	5.91E-6*EXP(-6160/TK)	6.2167E12*EXP(-8886/TK)
part4	1.259E-5*EXP(-6230/TK)	6.2167E12*EXP(-9095/TK)
part5	3.309E-5*EXP(-3030/TK)	6.2167E12*EXP(-9507/TK)
part6	5.353E-5*EXP(-6209/TK)	6.2167E12*EXP(-10200/TK)
part7	2.904E-5*EXP(-5940/TK)	6.2167E12*EXP(-8455/TK)
part8	1.245E-2*EXP(-7070/TK)	6.2167E12*EXP(-11564/TK)
part9	3.737E-2*EXP(-7250/TK)	6.2167E12*EXP(-12039/TK)

Ultimately, since the method to calculate boiling points of each species is based on approximate values for each functional group, both β and E_a are just estimations. It should be noted that experimental values for k_{on} and k_{off} can be one or two orders of magnitude higher than theoretical calculations, and that these are just estimations. To fit the model, these values could be adjusted within a reasonable range. In this case, just the values inside the exponential were adjusted so the model fit experimental data. In data analysis with this new model, total suspended particulates now includes part through part7, which were part of the original mechanism, as well as the newly added part8 and part9. Seed and seed1, the oligomer product, are also included in this value.

Chapter IV

RESULTS AND DISCUSSION

α-Pinene + NO_x Gas-Phase Mechanism Simulations and Comparisons

A total of thirteen experiments were modeled for testing the gas-phase α-pinene oxidation mechanism and included α-pinene alone or mixed with toluene and/or HCMix. All of the experiments are listed below in Table 5. Table 6 shows the initial conditions for two experiments from 1999 which were used to develop the original mechanism. Experiments included initial α-pinene concentrations ranging from 0.005 to 0.5 ppmV α-pinene, and initial NO_x concentrations ranging from 0.1 to 0.3 ppmV. All experiments with toluene used 0.143 ppmV toluene as the initial concentration, and all experiments with HCMix started with 3 ppmC HCMix. The experiments in this study are split into three categories: 1) α-pinene and NO_x only; α-pinene, 2) toluene, and NO_x; and 3) α-pinene, toluene, HCMix, and NO_x. The experiments in both of these tables are ordered from lowest HC/NO_x ratio to highest HC/NO_x ratio. The HC/NO_x ratio is the ratio of initial concentration of α-pinene to initial mixing ratio of NO_x (NO + NO_2).

Table 5. Experiments Performed Over the Summer of 2009, 2010, and 2011

Expt #	Date	$[\alpha\text{-Pinene}]_0$ (ppmV)	$[\text{Toluene}]_0$ (ppmV)	$[\text{UNCMix}]_0$ (ppmC)	$[\text{NO}]_0$ (ppm)	$[\text{NO2}]_0$ (ppm)	Gas- or particle-phase data	HC/NO_x ratio
1	ST0409 N	0.005	0.1428	3	0.26	0.0928	Gas, particle	0.0141
2	ST0509 S	0.01	0.1428	3	0.27	0.0145	Gas, particle	0.0351
3	ST1010 N	0.04	0.1428	0.0	0.22	0.0032	Gas, particle	0.1792
4	ST1610 S	0.04	0.1428	3	0.19	0.0106	Gas, particle	0.1994
5	ST0110 N	0.04	0.1428	0.0	0.18	0.0045	Gas, particle	0.2168
6	AU0910 S	0.05	0.0	0.0	0.12	0.0031	Gas	0.4061
7	JL3010 S	0.05	0.0	0.0	0.1	0.018	Gas	0.4237
8	ST1510 N	0.1	0.1428	0.0	0.23	0.0032	Gas, particle	0.4288
9	MY1511 S	0.1	0.0	0.0	0.2	0.0064	Gas, particle	0.4844
10	MY2111 S	0.1	0.1428	0.0	0.19	0.0056	Gas, particle	0.5112
11	JL2410 S	0.1	0.0	0.0.	0.17	0.0008	Gas	0.5854
12	OC1810 S	0.3	0.0	0.0	0.27	0.0034	Gas, particle	1.0972
13	OC1810 N	0.5	0.0	3	0.28	0.0043	Gas, particle	1.7587

Table 6. Two experiments performed in 1999 used for development of original mechanism

Expt #	Date	$[\alpha\text{-Pinene}]_0$ (ppmV)	$[\text{Toluene}]_0$ (ppmV)	$[\text{UNCMix}]_0$ (ppmC)	$[\text{NO}]_0$ (ppm)	$[\text{NO2}]_0$ (ppm)	Gas- or particle-phase data	HC/NO_x ratio
14	OC3099 N	0.94	0.0	0.0	0.48	0.002	Gas, particle	1.9502
15	JN0999 N	0.98	0.0	0.0	0.43	0.002	Gas, particle	2.2685

The kinetics simulation package, MORPHO, was used to simulate these experiments with the updated mechanism, as well as with the original 2001 mechanism (Kamens et al., 2001). Ambient pressure was set to be equal to 1 atmosphere, or 101,325 Pascals. The output of each simulation included gas-phase concentrations of O_3, NO, NO_2, and HONO, among others. Real-time temperature was also a variable output at each time step. The output of each model simulation can be plotted against time and compared to data from the smog chamber.

The plots in Figure 2, with α-pinene concentrations ranging from 0.05 to 0.3 ppmV, give an idea of how the new UNC mechanism performs with only initial concentrations of α-pinene and NO_x. Comparing these figures, it seems that the model does a better job of predicting O_3 production at higher concentrations of α-pinene. While comparing these, it is

likely important to consider the initial HC/NO_x ratio. The initial HC/NO_x ratio is simply the ratio of initial α-pinene concentration to initial NO_x concentration. The experiments from Figure 2b, Figure 2c, and Figure 2d all had HC/NO_x ratios of approximately 0.5, while the experiment from Figure 2a had a HC/NO_x ratio of 1. This could be important, because the experiments with a HC/NO_x ratio of 0.5 underestimated O_3 production by approximately 50%. The experiment with the HC/NO_x ratio of 1 had a much closer estimation of maximum O_3 production, with the model estimating to about 80% of the data. The two experiments (Kamens et al., 2001) that the original mechanism was based on both had HC/NO_x ratios that were greater than 1 (2.26 and 1.95). One reason for the difference in O_3 production could be due to unknown α-pinene and NO chemistry. A HC/NO_x ratio of 0.5 means that the initial concentration of NO_x was twice as high as the initial concentration of α-pinene , while the HC/NO_x ratio of 1 means that initially NO_x and α-pinene were present in equal concentrations. Another reason for the difference in O_3 production could be an issue in the way which the model represents or deals with PAN chemistry. Differences in produced O_3 levels due to the effect of HC/NO_x ratios have been documented before, and a similar discrepancy exists in models as well (Zhang et al., 2011). In this case, a difference in NO or NO_2 chemistry, either not included in the model or not yet known, could explain the difference in O_3 production. Figure 3 shows similar plots for the same experiments, created using the original 2001 mechanism. The average relative error in O_3 production went from 33% using the original mechanism to 25% using the updated mechanism. The updated mechanism does well early in the experiment, around 11:00 am, when O_3 is still rising. The original mechanism predicts this increase in O_3 happening more slowly. The updated mechanism also does well with predicting NO_2 behavior. By comparing Figures 2 and 3, it is

clear that both the modified and original UNC mechanisms grossly underestimate O_3 as initial experimental α-pinene concentrations are reduced from 0.3 to 0.05 ppmC. It may be important to note that chemiluminescence-based O_3 monitors, like the one used for the experiments in this study, can be affected by concentrations of water vapor (Kleindienst et al., 1993), which can cause a positive increase in detected ozone. Although neither of these mechanisms predicts O_3 formation well, there does seem to be a difference between the two, with the updated mechanism predicting an O_3 formation that is on average 9% higher than that using the original mechanism.

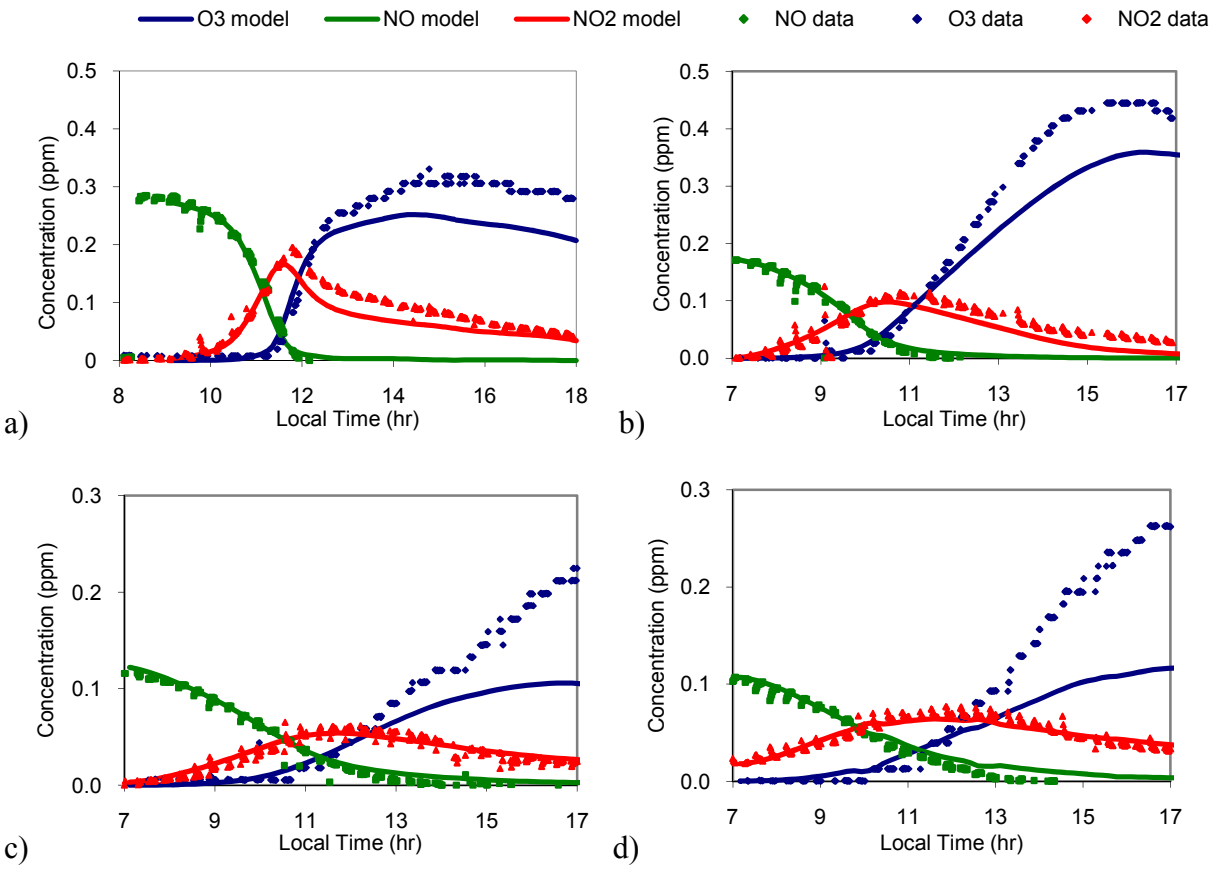

Figure 2. Model (lines) and data (points) gas-phase results of four α-pinene + NO_x experiments using the updated UNC mechanism. a) Experiment 12: 0.3ppm α-pinene + 0.3ppm NO_x, b) Experiment 11: 0.1ppm α-pinene + 0.2ppm NO_x, c) Experiment 6: 0.05ppm α-pinene + 0.1ppm NO_x, d) Experiment 7: 0.05ppm α-pinene + 0.1ppm NO_x.

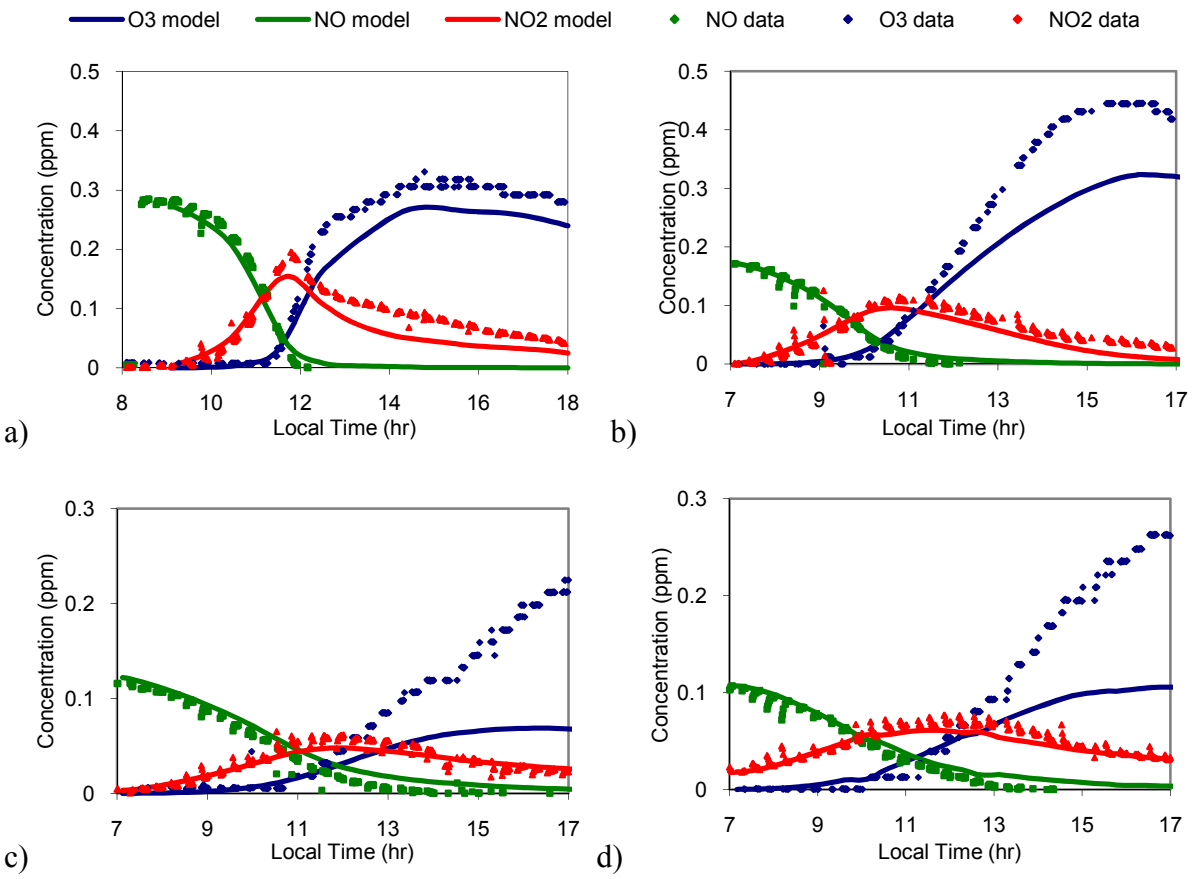

Figure 3. Model (lines) and data (points) gas-phase results of four α-pinene + NO_x experiments using the original 2001 mechanism. a) Experiment 12: 0.3ppm α-pinene + 0.3ppm NO_x, b) Experiment 11: 0.1ppm α-pinene + 0.2ppm NO_x, c) Experiment 6: 0.05ppm α-pinene + 0.1ppm NO_x, d) Experiment 7: 0.05ppm α-pinene + 0.1ppm NO_x.

To determine the extent to which significant changes influenced O_3 production, a sensitivity analysis was performed. Each change was made to the original mechanism individually, and a time plot of O_3 was produced to see the differences. The resulting O_3 curves for the two significant changes, along with the O_3 predictions of the original and final mechanisms, are plotted for one experiment below in Figure 4. This image shows that the change of acetone to PAR components and the addition of the organic nitrate decomposition reaction account for almost all of the increase in O_3 production from the original mechanism. These were the two modifications that caused the most significant changes in O_3 production.

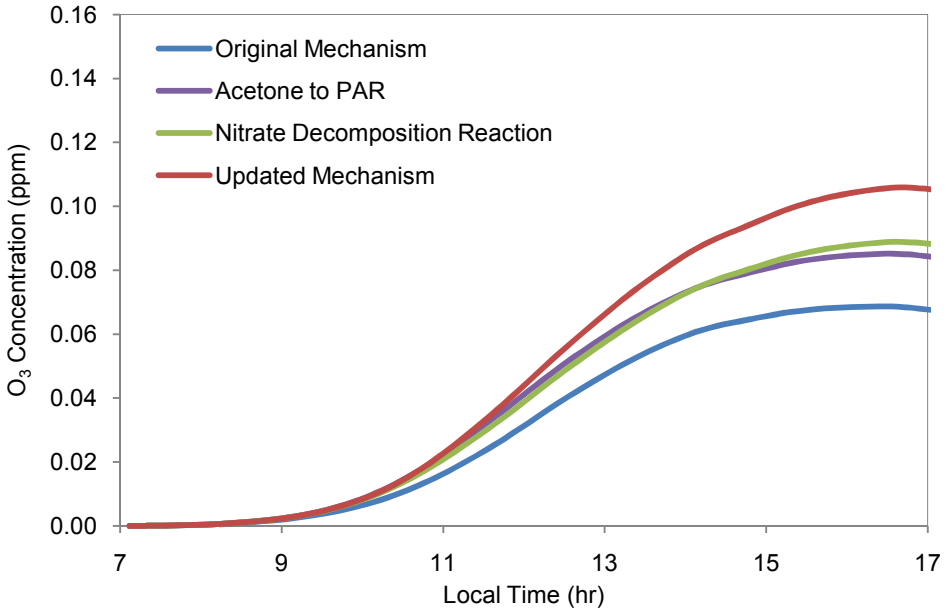

Figure 4. Sensitivity comparison of two major changes to mechanism for Experiment 6: the change from acetone to PAR and the addition of the nitrate decomposition reaction

Table 7. Sensitivity analysis: maximum O_3 with significant changes for Experiment 6

Change in Mechanism	**Maximum O_3 (ppm)**
Original mechanism	0.0687
Acetone to 3 PAR	0.0852
Addition of nitrate decomposition reaction	0.0888
Updated mechanism	0.106

Ultimately, the only way to produce O_3 is through photolysis and reaction of NO_2, HO_2, and RO_2s. RO_2 stoichiometric values cannot be changed, since a carbon balance needs to exist in each reaction. NO_2 can only be produced in a reaction which involves a nitrogen-containing compound. Stoichiometric coefficients for NO_2 cannot be changed unless there is an imbalance in nitrogen. Stoichiometric coefficients for HO_2 in a number of reactions were increased, and in some cases doubled or tripled, but this had little to no effect. Changes in products cannot be made just to increase O_3 production if they do not preserve a chemical

balance and if there is no data to suggest that the change might actually be occurring. This limits the number and types of changes that can be made.

The 2001 mechanism (Kamens et al., 2001) was originally based on two experiments from 1999, in which the initial α-pinene concentrations were just under 1 ppmV. Initial NO_x concentrations were between 0.4 ppm and 0.5 ppm. This 2001 mechanism reasonably modeled gas-phase chemistry from these 1999 experiments, but did slightly over predict O_3. Plots of the 1999 experiments and the model simulation produced by the updated mechanism (in MORPHO) can be found in Appendix C. Although the updated model comes close to what the 2001 version of the model, with another simulation package called PKSS, produced (Kamens et al., 2001), the initial concentrations of α-pinene in both these experiments are much higher than the experiments used in this work. From this, it is possible to conclude that the model from 2001 was built using high initial concentrations of α-pinene, and works best at those high concentrations. This mechanism, however, does not accurately predict O_3 production at lower α-pinene concentrations.

Simulations of α-Pinene with Toluene and HCMix

Figure 5 shows simulations of experiments which fall into two categories: α-pinene + toluene + NO_x (Experiment 5, Figure 5a), and α-pinene + toluene + HCMix + NO_x (Experiment 4, Figure 5b). From this figure, it can be seen that the mechanism predicts NO to NO_2 conversion fairly well, as both NO and NO_2 mechanism estimations fit NO and NO_2 experimental data. However, for experiments without initial injections of HCMix, the production of O_3 is almost always under predicted. On average, for experiments with toluene and HCMix, the mechanism is only predicting 85% of data O_3 production. Since the toluene

mechanism with HCMix present has been shown to accurately predict O_3 formation in the presence of the hydrocarbon mix, it is likely that the discrepancy in O_3 produced is due to inaccuracies in the α-pinene mechanism (Kamens et al., 2011). In general, the mechanism performs well with α-pinene and toluene, and the best with α-pinene and both toluene and HCMix. It is likely that the mechanism fits experiments that include HCMix because of the high concentration of HCMix compared to both toluene and α-pinene. In this situation, the chemistry of HCMix and its products would dominate that of toluene and α-pinene. It is possible that the production of more RO_2 radicals from HCMix would compete with RO_2 radicals produced from a-pinene for reactions with NO, leading the experiment to act more like one in which the HC/NO_x ratio is higher. Overall, the maximum O_3 simulation error for the UNC model for all experiments is between -54% and 25%. The only simulation with a positive relative error is OC1810N, which started with the highest initial α-pinene concentration in this study, and also included HCMix.

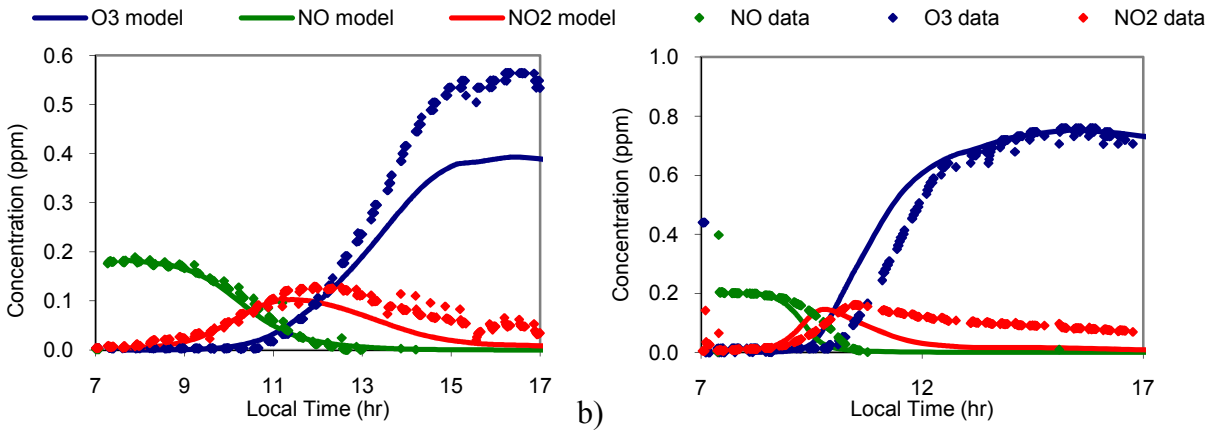

Figure 5. Model and data gas-phase results of experiments with α-pinene and toluene or HCMix using the updated UNC mechanism. a) Experiment 5: 0.04ppmV α-pinene + 0.1429ppmV toluene + 0.2ppm NO_x, b) Experiment 4: 0.04ppmV α-pinene + 0.1429ppmV toluene + 3ppmC HCMix + 0.2ppm NO_x

Inter-comparison of Common Mechanisms

The gas-phase portion of the UNC mechanism was compared with other commonly used mechanisms, including MCMv3.1, SAPRC07, and CB05. Time concentration profiles of O_3, NO, and NO_2 were generated for each experiment. The gas-phase concentration profiles from all four mechanisms for Experiment 12 are shown in Figure 6. Similar plots for each experiment were used to compare three factors: maximum O_3, NO-NO_2 crossover time, and the O_3 slope. Examples of the comparisons are shown below in Figure 7. As Figure 7a shows, the UNC mechanism did a reasonable job of predicting maximum O_3 production. It does, however, under predict O_3 for most experiments, as do CB05 and SAPRC07; MCMv3.1 was the only mechanism that over predicted O_3. The median of the relative errors was smallest for the UNC mechanism, at -25.6%. As CB05, SAPRC07, and MCMv3.1 do not represent particle-phase chemistry, these mechanisms did not account for ozone deposition onto particles. Ultimately, this decreases O_3 loss, which makes the mechanism appear as if it produces more O_3. This process, however, is represented in the UNC mechanism and essentially acts as a sink for O_3.

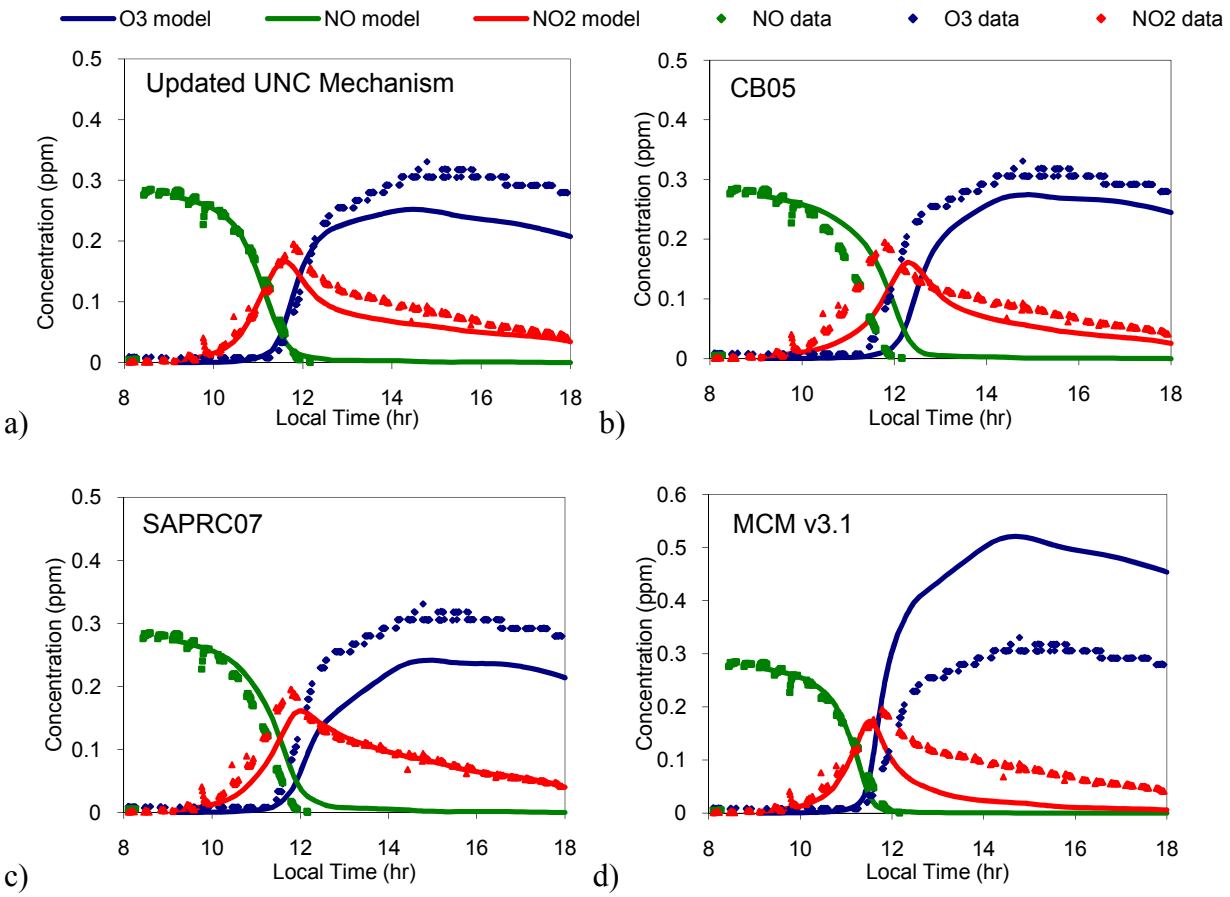

Figure 6. Gas-phase model performances for Experiment 12 using a) updated UNC mechanism, b) CB05, c) SAPRC07, and d) MCMv3.1

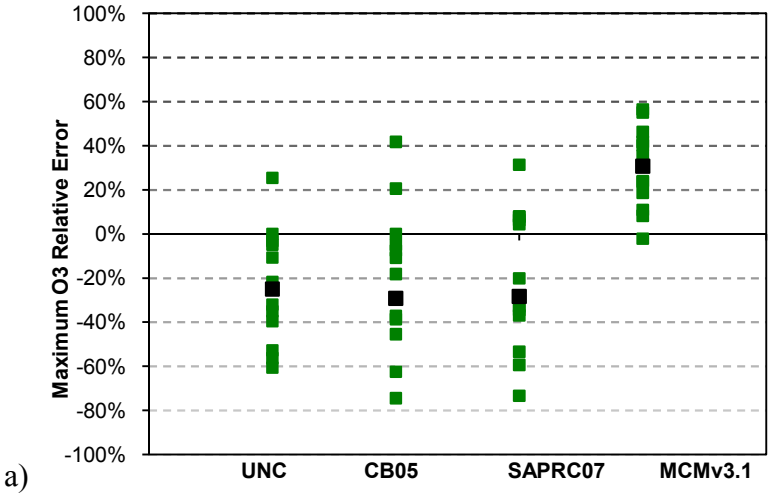

a)

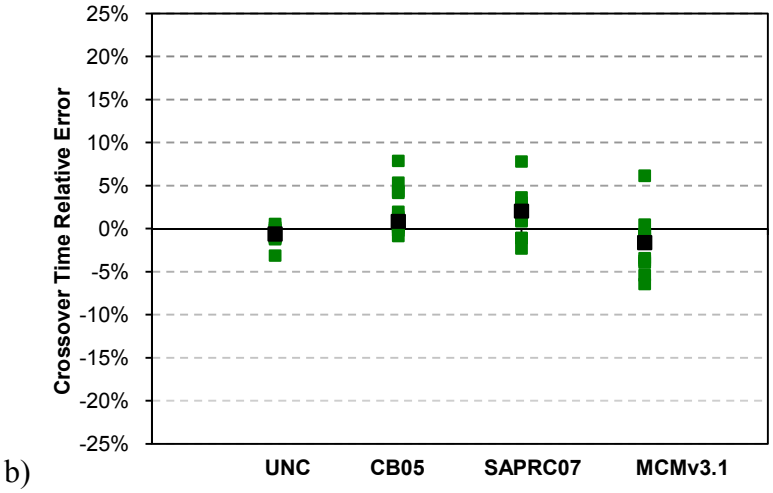

b)

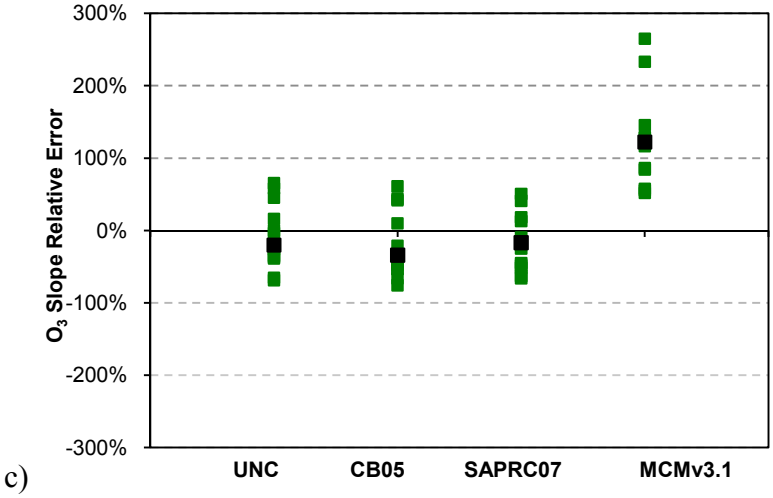

c)

Figure 7. Relative errors of UNC mechanism and 3 other commonly used mechanisms. Relative errors for individual experiments (green) and mean relative errors (black) for a) maximum O_3 measurements b) NO-NO_2 crossover time, c) O_3 slope.

The UNC mechanism performs better for the NO-NO_2 crossover and O_3 slope metrics than the other mechanisms as well. The NO-NO_2 crossover time gives an idea of how fast the conversion of NO to NO_2 is occurring, which gives an overall idea for the speed of the mechanism. For NO-NO_2, a positive relative error means that the model crossover time is later than the data, and a negative relative error means that the model time is earlier than the data. The median values for the UNC mechanism are closest to zero for crossover time. This is expected, since all initial HONO concentrations were set to the level that was optimal for the UNC mechanism. There were a few cases for which the UNC mechanism had too fast of a conversion of NO to NO_2, which is seen by the negative relative errors in Figure 7b. For those simulations in which the NO-NO_2 crossover time was occurring to quickly, HONO had already been reduced to an initial concentration of zero. The O_3 slope metric is the slope of the initial rise in O_3. From Figure 7c, MCMv3.1 is estimating the rate of O_3 production to be too high, while the other three mechanisms perform similarly predicting the rise is O_3 a little more slowly.

In general, it seems as if the UNC mechanism and MCMv3.1 do the best job out of the four mechanisms of predicting O_3 production and representing NO to NO_2 chemistry. The UNC mechanism performed best for the simulations including HCMix. On the other hand, MCMv3.1, best predicted maximum O_3 in those experiments, which had only α-pinene and toluene as initial hydrocarbons. With the inclusion of HCMix, MCMv3.1 started to over predict O_3 production by 30%, on average.

Particle-Phase Mechanism Comparison

All experiments except for numbers 6, 7, and 11 had particle-phase data available through an SMPS system, and particle production was modeled with the UNC mechanism. In all figures, the model output value of total suspended particulates (TSP) is equal to the sum of individual particle-phase products (called 'part' through 'part7', includes 'part8' and 'part9' for updated mechanism), along with seed (initial background seed) and seed1 (oligomer products). In all simulations, background aerosol was represented in the model as an initial injection of seed, allowing for a surface for initial partitioning. This initial value was adjusted to match the background seed concentration from DMA data. The original UNC mechanism (Kamens et al., 2001), as shown in Figure 8 for the simulations OC1810N and OC1810S, did not fit data at lower α-pinene concentrations. Although the original 2001 UNC mechanism estimated SOA production accurately 1999 experiments (Kamens et al., 2001), it underestimated the total amount of SOA produced by the experiments performed more recently, all of which had lower concentrations of α-pinene. Figures 9 and 10, below, show how the updated UNC mechanism fit particle-phase data. In all cases, initial seed was between 3.5 $\mu g/m^3$ and 35 $\mu g/m^3$.

The experiments OC1810N and OC1810S were modeled using the original mechanism, and as shown in Figure 8, the original mechanism failed to capture the trend of the data. The updated mechanism, shown in Figure 9, did a better job at capturing this and fitting α-pinene + NO_x data. In Figure 9b, the updated mechanism actually overestimates O_3 production. As discussed later, the updated model creates a significant amount of 'pinald-PAN', which is the PAN-like product created from α-pinene. The production of this nitrogen-containing product includes reactions with NO_2, so the production of 'pinald-PAN' will be

greater when initial NO_x concentrations are high compared to hydrocarbons, or when the HC/NO_x ratio is low. This means that it fits most of the experiments in this data set, but could overestimate SOA production in scenarios where PAN, and NO_x chemistry in general, is working under different conditions. Figure 10 shows that the updated UNC model also fits particle phase data well for a variety of conditions. The scales for each plot in this figure have been adjusted to fit the data. The immediate initial jump in SOA growth in the model is due to water uptake on background seed particles in the toluene mechanism. The evaporation of this particle-phase water as the temperature rises in the morning is depicted in the data as the drop in TSP, and this is captured by the model. Additionally, in most cases, the model captured the particle loss in the evenings which is likely due to particle losses to the walls. The increase in TSP in the Figure 8, modeled using the original mechanism, is unintentional and thought to be an error in how the solver sums this particular value. Ideally, the value of TSP should decrease after reaching the maximum value. TSP is properly depicted in Figure 9. A solver error also is the cause of the bump in estimated TSP in Figure 10b.

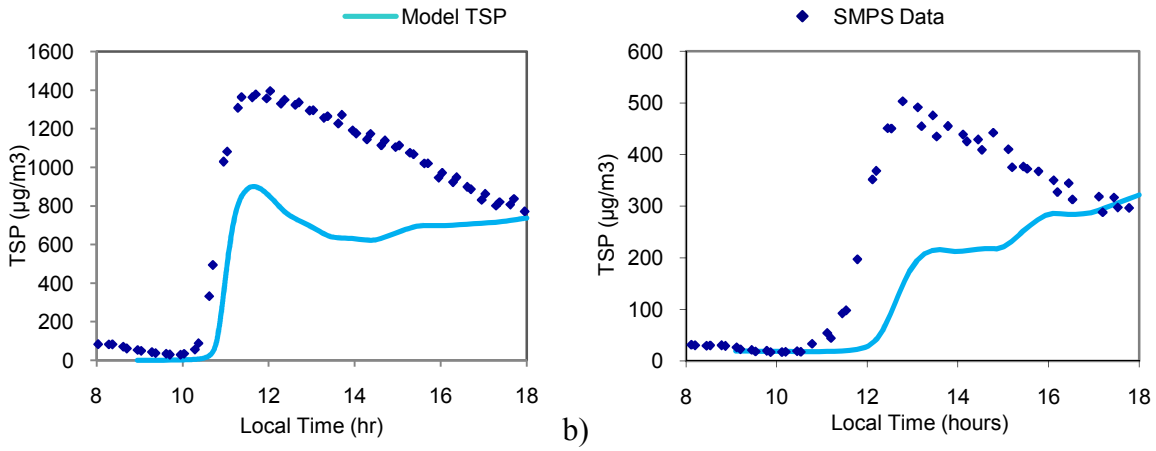

Figure 8. Model (lines) and data (points) particle-phase results using the original 2001 mechanism for a) Experiment 13: 5ppmC α-pinene + 3ppmC HCMix + 0.3ppm NO_x and b) Experiment 12: 3ppmC α-pinene + 0.3ppm NO_x.

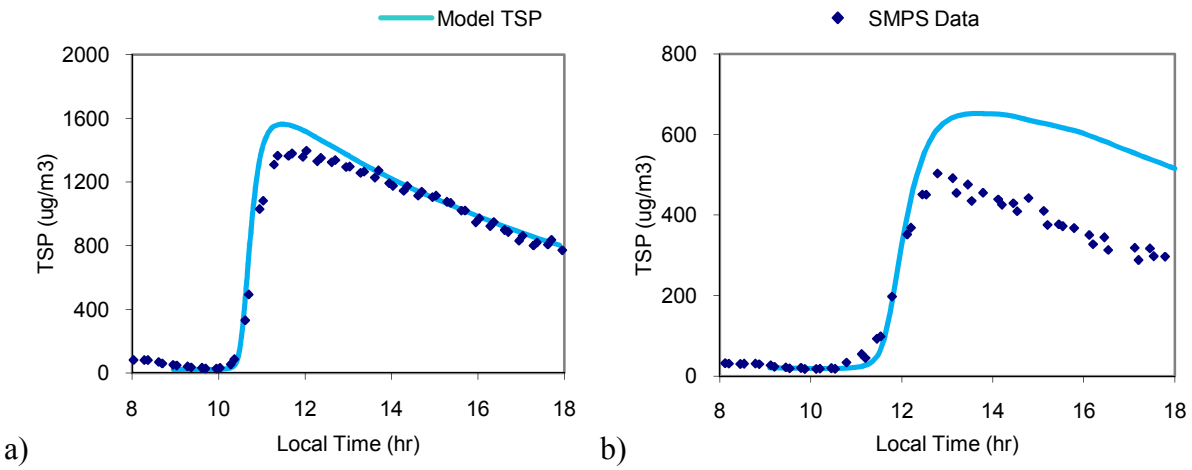

Figure 9. Model (lines) and data (points) particle-phase results using the updated UNC mechanism for: a) Experiment 13: 5ppmC α-pinene + 3ppmC HCMix + 0.3ppm NO_x and b) Experiment 12: 3ppmC α-pinene + 0.3ppm NO_x

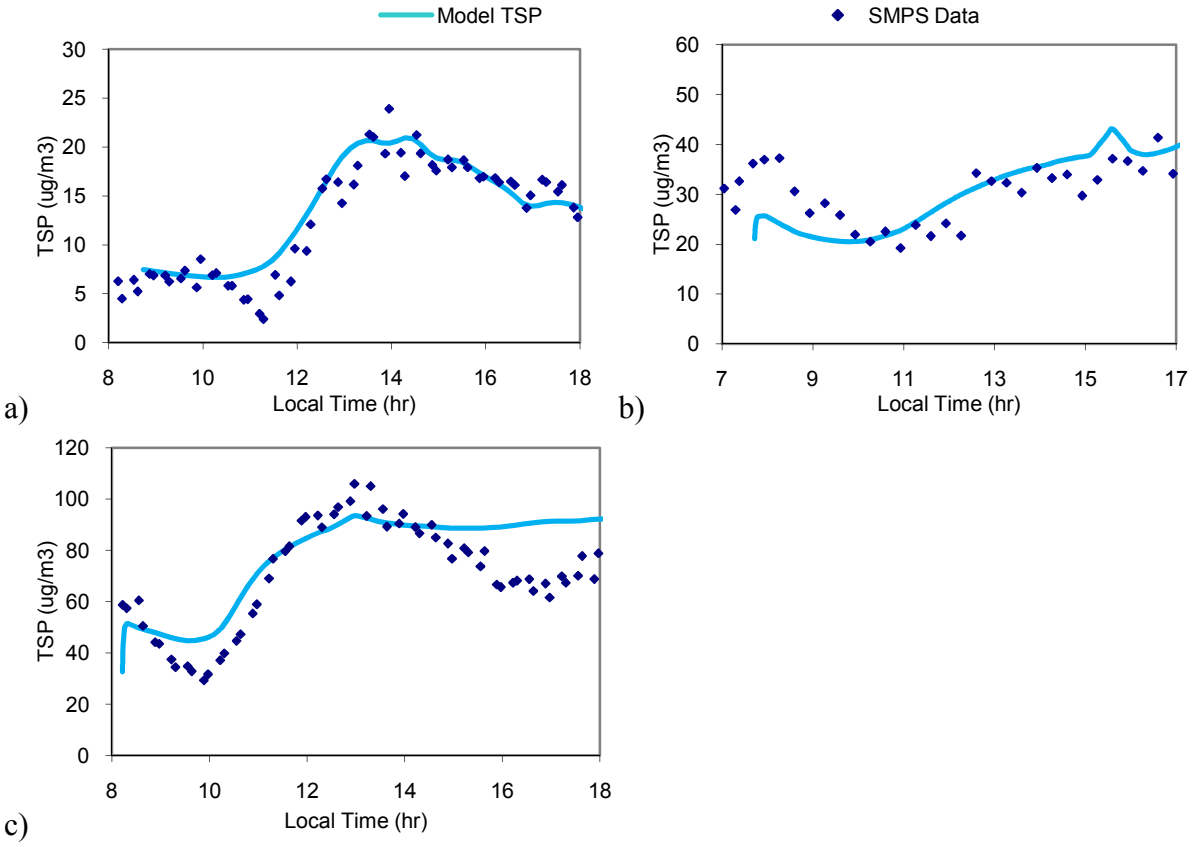

Figure 10. Model (lines) and data (points) particle-phase results of experiments with different initial conditions using the updated UNC mechanism for a) Experiment 9: 0.1ppmV α-pinene + 0.2ppm NO_x, b) Experiment 5: 0.04ppmV α-pinene + 0.1429ppmV toluene + 0.2ppm NO_x, c) Experiment 4: 0.04ppmV α-pinene + 0.1429ppmV toluene + 3ppmC HCMix + 0.2ppm NO_x

The updated UNC mechanism was also used to model the SOA produced from the experiments from 1999, with the general result of over predicting SOA production. The results of these two simulations can be seen in Appendix C. It is possible that SOA is over estimated for these experiments because of a discrepancy with the way the model works. The high concentration of hydrocarbons compared to NO_x means that RO_2 chemistry will predominate, leading to the production of more SOA as expected. For the cases in this data set, the chemistry of NO_x and RO_2 is more predominant than that of RO_2 cross reactions. These scenarios are different for different HC/NO_x ratios and this could be a reason why each model only fits a certain data set.

Simulation of α-pinene Particle-Phase Products

Filter samples from Experiments 12 and 13, on October 18th, 2010, were extracted and analyzed by GC/MS. No prior derivatization of the filter extracts was employed in this method. Pinonic acid, a product of α-pinene oxidation, was used as a standard. Two filter samples were taken, each for two hours, at different times during the day. The filter samples gave an average mass concentration of particle-phase pinonic acid produced over those two hours. From the mass spectra of pinonic acid standards, it was determined that this species eluted between 13.7 and 14 minutes. A total ion chromatogram (TIC) for the second filter pulled from the North side is shown in Figure 11. The pinonic acid peak is labeled. Pinonic acid concentrations on each filter were determined by the ion at mass 83, an ion characteristic to this species (Jaoui et al., 2001). The efficiency of the extraction method described in the Methods section was approximately 33%. A description of the determination of extraction efficiency can be found in Appendix A.

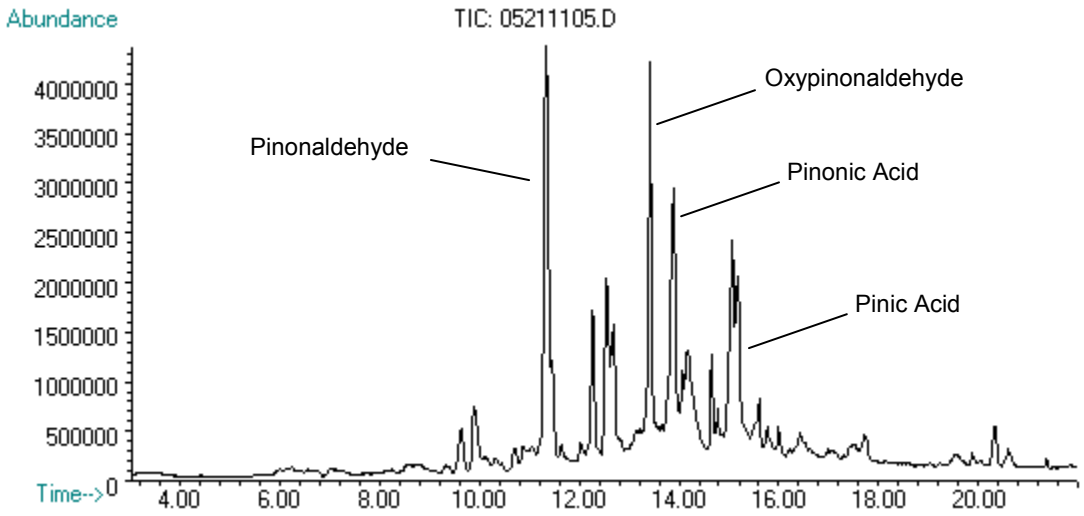

Figure 11. GC/MS TIC for Experiment 13 Filter 2 with pinonic acid, pinic acid, pinonaldehyde, and oxypinonaldehyde peaks labeled.

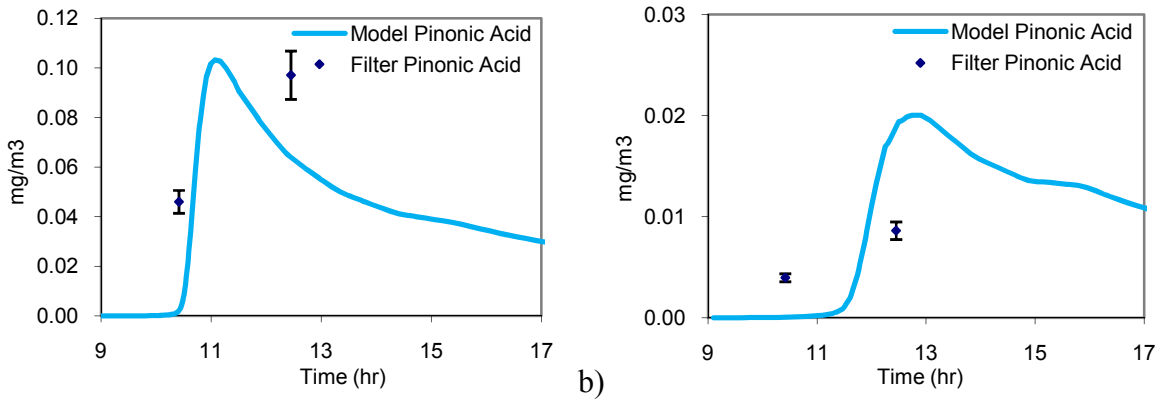

Figure 12. Data (symbols) and model estimations (lines) of particle phase pinonic acid from aerosol filter samples for a) Experiment 13 and b) Experiment 12.

The results for these experiments are shown in Figure 12. Each point represents the mass concentration from the filter. For both filters, average mass concentration of pinonic acid was set to the midpoint of the time period during which the filters were pulled. As these are average times, and aerosol concentration changed quickly over both time periods, there may be errors associated with the point in time at which each measurement was assigned.

Error bars for the measurements of mass concentration for each filter also have associated errors, shown by the error bars. The percent error is a combination of the following: error in the sample pump volume used for obtaining the filter sample (±10%, 2 standard deviations), error in the balance used to measure filter masses (±1%), error in the GC/MS, determined from the error in pinoinc acid standards (±0.26%). The reasonable closeness of the filter data to the model, with associated errors, lends some validity to the updated particle-phase model; however, more filter samples from different time points are needed to fully evaluate the performance of the particle-phase model output.

Although standards were not available for other significant α-pinene oxidation products, relative retention times based on previous work (Jaoui et al,. 2001) could be determined in relation to the pinonic acid peak in that work. Relative retention times, or the ratio between two peaks, will be approximately the same for every chromatogram. Retention times are dependent upon volatility, so relative times of elution will be the same for each chromatogram. Using these relative retention times, elution times for a few other products could be calculated, based on the known elution time for the pinonic acid peak. Using this method, and their respective mass spectra, the following peaks were identified: pinic acid, pinonaldehyde, and oxypinonaldehyde. While we cannot determine average concentrations for these species, it is significant to know with certainty that each of these species were also produced. This at least allows some confidence in knowing that these products were actually produced and in amounts relatively close to what the model suggests.

A plot of the products from an experiment, in this case experiment number 13, gives some insight into how the model is predicting particle-phase products. This plot is shown below in Figure 13. This simulation is producing over two times as much pinald-PAN as the

next highest product created. Pinald-PAN is the peroxyacyl nitrate product produced from α-pinene photo-oxidation. These compounds are very similar to peroxyacetyl nitrate (PAN), in that they are a reservoir for NO_2, and at high temperatures will dissociate into an RO_2 radical and NO_2. This is a significantly higher amount of pinald-PAN produced than the 1999 experiments (Kamens et al., 2001). The change in pinald-PAN production is due to adjusting the exponential portion of partitioning rates in the mechanism. This value was changed by less than 10%. It is difficult to determine whether or not the model estimations are accurate since PANs will decompose to an RO_2 and NO_2 at high temperatures. The GC has an FID and the GC-MS has an EI source, both of which exceed the temperature at which PAN-like products start to dissociate, making it difficult to determine real-time concentrations of these compounds. Every experiment modeled in this work showed the same trend of having high production of PAN-like species, this does not hold only for experiments with high HC/NO_x ratios.

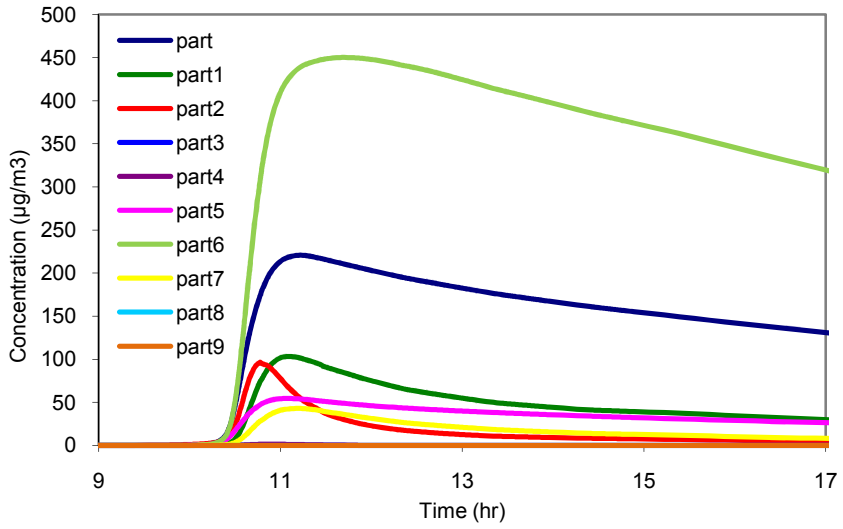

Figure 13. Prediction of particle-phase products from Experiment 13.

To determine the effect that these changed partitioning rates had on pinald-PAN and total SOA production, rates of partitioning to and from the particle phase were both adjusted until SOA production for the 1999 experiments was much closer to total mass as determined by filters. The same mechanism with adjusted partitioning rates was used to model a few α-pinene + NO_x experiments, and while pinald-PAN production was decreased, SOA had decreased more than expected. Additionally, more gas-phase pinald-PAN means there will be more NO_2 available, since pinald-PAN will decompose over the course of the afternoon when temperatures are high enough. The additional available NO_2 will increase O_3 production throughout this period of time. While these partitioning rates meant that model SOA had a closer fit to 1999 SOA data, the model was over predicting O_3 even more. The 1999 experiments modeled with the updated mechanism were already over predicting O_3. This shows that there may be different PAN and, indirectly, NO_2 chemistry between the two cases. There may a HC/NO_x influence on α-pinene atmospheric chemistry, in that different chemistry dominates when there is an excess of NO_x or NO_x is limiting, which is consistent with work by Ng et al. (2007).

Chapter V

SUMMARY AND CONCLUSION

In this paper, an updated version of UNC's α-pinene photooxidation model is presented. Changes to the mechanism include the inclusion of newly discovered α-pinene products and updated rate constants. Partitioning from gas to the particle phase was also updated, and partitioning for the new gas-phase products was included. To evaluate this model, a series of 13 outdoor chamber experiments were performed over three summers for experimental data. A number of these experiments include toluene, an important anthropogenically created VOC, and HCMix, a mix of common hydrocarbons. The purpose of including both toluene and HCMix was to simulate α-pinene chemistry in an urban environment, an issue which is becoming of greater importance, and to investigate SOA formation from α-pinene in the environment of another SOA forming hydrocarbon. In the case where toluene was also introduced initially to the chamber, the recently published toluene gas and particle-phase mechanism from Kamens et al. (2011) was used to simulate products. This mechanism includes both gas- and particle-phase products. Important gas-phase species include O_3, NO, and NO_2. α-Pinene particle-phase products are split up into 9 species, and are combined, along with background seed aerosol and oligomer products, to give the value of TSP. When toluene was also an initial hydrocarbon, particle-phase products from the toluene mechanism were also included in TSP.

The mechanism simulates O_3 production and NO-NO_2 conversion fairly well. In cases of a low HC/NO_x ratio (where initial NO is much greater than initial α-pinene), the

mechanism predicts only 50% of O_3 production. This shows that there may be a difference in RO_2 chemistry when NO and NO_2 are in excess. In the presence of HCMix, the mechanism does very well, only under predicting ozone by 4.7%, on average. The accuracy of this mechanism within the hydrocarbon mixture suggests that it may be have potential uses in simulating complicated atmospheric chemistry. However, it is possible that RO_2 cross reactions dominate in the presence of HCMix, because of its high concentration compared to both toluene and α-pinene. The RO_2 chemistry of HCMix is not described in as much detail as that of toluene and α-pinene, because HCMix components were inputted in CB05 terminology, which includes limited RO_2 chemistry.

An inter-comparison of the gas-phase mechanism was performed with three other common atmospheric chemistry mechanisms, CB05, SAPRC07, and MCMv3.1. For each of the four mechanisms, three metrics were used to determine accuracy: maximum O_3, NO-NO_2 crossover time, and O_3 slope. Overall, the UNC Mechanism performed the best for this set of experiments. In general, MCMv3.1 overproduced O_3, had too fast of an NO-NO_2 crossover time, and estimated the O_3 production as increasing too quickly. SAPRC07 and CB05 both under predicted O_3 production even more than the UNC mechanism, and converted NO to NO_2 slower than the UNC mechanism.

It seems possible that the UNC mechanism (as well as CB05 and SAPRC07) is missing a few crucial reactions involving NO and NO_2. When initial NO_x concentrations were high compared to initial α-pinene concentrations (a low HC/NO_x ratio), the mechanism did a poorer job predicting maximum O_3 production. As the HC/NO_x ratio increased, the mechanism did a better job. However, only with the inclusion of HCMix did the UNC mechanism fit maximum O_3 well. This is likely due to the production of small RO_2 radicals

from HCMix, which will make RO_2 radical cross reactions more dominant than RO_2 radical reactions with NO. It is possible that under different HC/NO_x ratios, or NO regimes, the dominant chemistry of RO_2 radicals, NO, NO_2, and HO_2 is different. This would account for the different model performances under different initial conditions.

The particle-phase portion of the mechanism was used to simulate total particle production for the ten experiments in which DMA data was available. The mechanism did a good job of estimating total aerosol production. Filter samples from one experiment were used to quantify the average mass concentration of pinonic acid, an important gas and particle phase product of α-pinene photooxidation, over time periods of two hours. Results from the filters showed that the particle-phase mechanism may predict particle-phase pinonic acid well; however, higher time resolution data for this compound is needed in order to validate the quality of this component of the model. Comparison to the other commonly used mechanisms was not possible, since they do not represent particle-phase chemistry.

This work may have greater implications because the α-pinene mechanisms investigated here are used commonly in air quality models. The under prediction of O_3 by most models at low α-pinene concentrations means that these models will under predict O_3 at concentrations that are more atmospherically relevant, since these are lower than most concentrations used in this study. The UNC mechanism may not be ready for use in air quality models, and based on the comparison with other commonly used mechanisms, it may not be a good idea to use either CB05 or SAPRC07 to predict O_3 production from α-pinene at low concentrations. Both of these have the same issue of predicting a slow rise in O_3 concentration and under predicting maximum O_3 production. All of these mechanisms are currently in use, so this comparison could have more immediate implications.

Chapter VI

RECOMMENDATIONS

Accurate models of atmospheric chemistry are important to be able to correctly predict O_3 and SOA formation for health and policy uses. This model of α-pinene atmospheric reactions, and testing with the available database of experiments, shows that while the total aerosol product is accurately represented, there are inaccuracies in O_3 predictions. The model does a better job at predicting O_3 when initial α-pinene concentrations are high (or at higher HC/NO_x ratios). To get a better understanding of this, a more complete database should be compiled for testing with a variety of mechanisms, to determine if this trend holds for a wider range. Further work should be done to determine product composition and concentration for experiments with lower initial α-pinene concentrations. These products should include the significant α-pinene products as well as PAN, as PAN production will be a consequence of the level of NO_2 present. Determining if the discrepancy is due strictly to lower initial α-pinene concentrations or simply to a lower initial HC/NO_x ratio would be beneficial.

From the work here, it seems that the model is unable to accurately predict O_3 production at lower HC/NO_x ratios. Further exploration should be done to determine why this is the case. With the inclusion of HCMix, the model performs significantly better, likely because of the influence of RO_2 chemistry. A more explicit method of inputting HCMix components into the mechanism may show how these components influence O_3 production, and the subsequent effects that this mix has on SOA production. It may also be helpful to

look at model budgets of radicals such as OH, HO_2, and RO_2s. Investigating these radicals throughout each experiment will give more insight into the extent that each radical reacts with other species as well as more information about how they terminate. Special attention should be given to how these radicals behave at times later in the day when estimated O_3 concentrations deviate from experimental O_3 data. With some insight into how each of these radicals behaves over the course of the day and for a series of initial conditions, a more detailed and comprehensive gas-phase model can be developed.

It is possible that unknown chemistry dominates when there is an excess of NO_x or some other unknown experimental artifact that is not yet included in the UNC mechanism. Since MCMv3.1 did over-predict O_3 in most cases, there is a chance that this mechanism includes the additional chemistry that is not included in the UNC mechanism. Going through this mechanism to determine which reactions cause the greatest increase in O_3 could be beneficial to improve the UNC mechanism. It is also possible that the chemistry in question is unknown, in which case further experimentation would be necessary to determine those reactions.

APPENDICES

APPENDIX A: Explanation of Extraction Efficiency

The extraction efficiency for the method of extraction described in the Methods section was determined for three compounds of different volatility. This included the two internal standards, bornyl acetate and methyl tridecanoate, as well as pinonic acid. GC/MS analysis of the filters, which contained both internal standards, showed no bornyl acetate peaks; if they were there, they were indiscernible from background organics. This was troubling because that meant it had likely volatilized during the process of blowing down the methanol solvent under N_2 at ambient temperatures. To determine the amount of each internal standard and pinonic acid that was being blown off, three blank filters were spiked with known concentrations of the internal standards and pinonic acid, put through the same extraction process, and analyzed using the GC/MS. Previous standard curves of both internal standards and pinonic acid, made from pure compounds in acetonitrile, were used to determine the concentrations from the GC/MS peak areas. Knowing the initial amount on the filter, the final concentration in the GC vial with 100% extraction efficiency could be calculated. From this, a value for the amount of each compound lost could be determined; the percent remaining would be the extraction efficiency.

A plot of extraction efficiency, which is the percent remaining after extraction, against elution time, shows a linear relationship between the two. Each point is an average of the results from three blank filters. Since elution time is directly related to volatility, it is likely that the method of blowing the methanol solvent dry was the reason for the very low extraction efficiency for earlier eluting compounds.

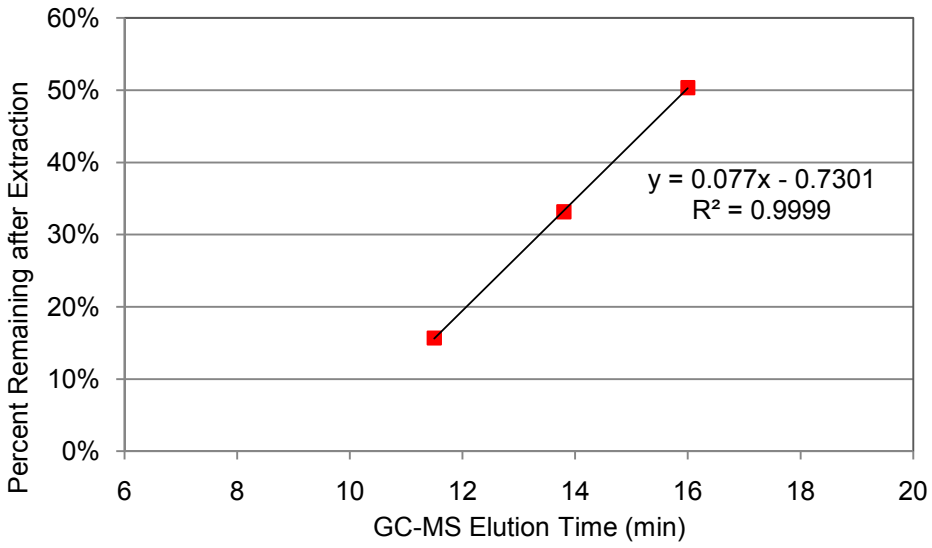

Figure A-1. Extraction efficiencies of extraction procedure used in this work based on elution time from GC/MS

APPENDIX B: Additional Tables and α-pinene Mechanism

Tables

Table B-1. Major gas-phase products

apine	α-pinene
C2O3	Acetylperoxy radicals
C8O2	Eight carbon peroxy radicals
diacid	Pinic and norpinic acid
OH-apNO3	α -pinene nitrate products
OH-apN2O6	α -pinene dinitrate products
oxypinacid	Oxo-substituted pinonic acids
oxypinald	Oxo-substituted pinonaldehyde
pinacid	Pinonic and norpinonic acid
pinald	pinonaldehyde
pinald-PAN	Pinonaldehyde-based PAN products
pinalic	Pinalic acid
pre-tri	Tri-carboxylic acid precursor to part8
stabcrieg1 and stabcrieg2	Stabilized criegee radicals
vol-oxy	Oxygenated, low vapor pressure products

Table B-2. All particle-phase products

seed	Background aerosol, average MW = 120 g/mol
seed1	Oligomer products, average MW = 362 g/mol
part	Diacid – pinic and norpinic acid, average MW = 186 g/mol
part1	Pinonic and Norpinonic acid, average MW = 184 g/mol
part2	Pinonaldehyde, MW = 168 g/mol
part3	Oxy-substituted pinonaldehyde, MW = 184 g/mol
part4	Pinalic acid, MW = 172 g/mol
part5	Oxy-substituted pinacids, average MW = 200 g/mol
part6	Pinald-PAN, MW = 245 g/mol
part7	α-pinene nitrates, MW = 201 g/mol
part8	3-Methyl-1,2,3-butane-tricarboxylic acid, MW = 217 g/mol
part9	α-pinene dinitrate, MW = 273 g/mol

α-pinene Mechanism

NAMES

```
PhotoRateIDs += { pinald_to_pinO2, COOH_to_HO2, OXYPINALD_to_OXYPINO2, pinalic_to_P3O2 };

// {Gas-phase Reactions}
R[AP_1] = apine + OH  ----> 'ap-oo'                                                                          @1.2E-11*EXP(440/TK);
R[AP_2] = 'ap-oo' + NO ----> 0.77*NO2 + 0.52*pinald + 0.85*HO2 + 0.25*XO2 + 0.18*FORM + 0.23*'OH-apNO3'
                             + 0.195*PAR + 0.18*'vol-oxy'                                                    @4.10E-12*EXP(180/TK);
R[AP_3] = apine + NO3 ----> 'apNO3-oo'                                                                       @1.2E-12*EXP(490/TK);
R[AP_4] = 'apNO3-oo' + NO ----> 0.81*NO2 + 0.19*'OH-apN2O6'+ 0.81*'OH-apNO3' + 0.81*HO2                      @4.10E-12*EXP(180/TK);
R[AP_5] = apine + O3 ----> 0.4*crieg1 + 0.6*crieg2                                                           @1.01E-15*EXP(-732/TK);
R[AP_6] = crieg1 ----> 0.49*pinacid + 0.13*stabcrieg1 + 0.8*OH + 0.3*HO2 + 0.39*pinald + 0.01*oxypinald
                       + 0.03*O3P + 0.19*CO + 0.07*'vol-oxy'                                                 @1.67E4;
R[AP_7] = crieg2 ----> 0.4*crgprod2 + 0.08*oxypinald + 0.433*'vol-oxy'+ 0.13*stabcrieg2 + 0.8*OH + 0.3*HO2
                       + 0.03*O3P + 0.4*FORM + 0.12*pinacid                                                  @1.67E4;
R[AP_8] = stabcrieg1 + H2O ----> pinacid                                                                     @3.66E-17;
R[AP_9] = stabcrieg2 + H2O ----> 0.7*pinalic + 0.3*pinald + H2O2                                             @3.66E-17;
R[AP_10] = stabcrieg1 + NO ----> pinald + NO2                                                                @7.00E-12;
R[AP_11] = stabcrieg1 + NO2 ----> NO3 + pinald                                                               @1.001E-13;
R[AP_12] = stabcrieg2 + NO ----> pinald + NO2                                                                @7.00E-12;
R[AP_13] = stabcrieg2 + NO2 ----> NO3 + pinald                                                               @1.001E-13;
R[AP_14] = crgprod2 + HO2 ----> 0.8*diacid + 0.2*oxypinacid                                                  @4.30E-13*EXP(1040/TK);
R[AP_15] = O3P + apine ----> 0.6*'vol-oxy' + 0.4*HO2 + 0.2*oxypinald + 0.26*pinald                           @1.19E-11*EXP(-324/TK);
R[AP_16] = 'ap-oo'  + HO2 ----> 0.5*'ap-ooH' + 0.5*'vol-oxy' + OH                                            @2.60E-13*EXP(1250/TK);
R[AP_17] = 'ap-ooH' + OH ----> 'ap-oo' + H2O                                                                 @1.92E-12*EXP(190/TK);
R[AP_18] = 'ap-ooH'  ----> 'ap-oo' + OH + 0.15*'pin-ooH'                                                     @ j[COOH_to_HO2];
R[AP_19] = 'apNO3-oo' + HO2 ----> 'OH-apNO3'                                                                 @2.65E-13*EXP(1300/TK);

R[AP_20] = pinald ----> 0.7*pinO2 + 1.3*CO + 1.6*HO2 + 0.3*C8O2 + 0.6*XO2                                    @j[pinald_to_pinO2];
R[AP_21] = pinO2 + NO ----> 0.765*pinald + 0.9*HO2 + 0.865*NO2 + 0.135*'OH-apNO3' + 0.015*XO2                @4.10E-12*EXP(180/TK);
R[AP_22] = C8O2 + NO ----> 0.84*NO2 + 0.711*'vol-oxy' + 0.8*HO2 + 0.16*'OH-apNO3' + 0.04*XO2                 @9.10E-12*EXP(180/TK);
R[AP_23] = pinald + OH ----> 0.8*'pinald-oo' + 0.1*C2O3 + 0.3*PAR + 0.1*C8O2 + 0.3*XO2                       @3.9E-11;
R[AP_24] = 'vol-oxy' + OH ----> 1.5*PAR +  0.3*C2O3 + 1.3*XO2 + 0.5*C8O2                                     @6.77E-12;
R[AP_25] = pinacid + OH ----> C2O3 + 1.5*PAR + 1.3*XO2 + 0.5*C8O2                                            @8.80E-12;
R[AP_26] = pinald + NO3 ----> 0.8*'pinald-oo' + 0.3*PAR + 0.3*XO2 + 0.1*C2O3 + 0.1*C8O2 + HNO3              @2.0E-14;
R[AP_27] = 'pinald-oo' + NO ----> pinO2 + CO2 + NO2                                                          @7.15E-12*EXP(290/TK);
R[AP_28] = 'pinald-oo' + NO2 ----> 'pinald-PAN'                                                              @2.63E-12*EXP(380/TK);
R[AP_29] = 'pinald-PAN' ----> 0.95*'pinald-oo' + 0.015*'oxypin-oo' + 0.035*'predi-oo' + NO2                  @1.78E9*EXP(-8459/TK);
R[AP_30] = 'pinald-PAN' + OH ----> PAN + C8O2                                                                @8.80E-12;
```

R[AP_31] = 'pinald-oo' + HO2 ----> 0.4*pinacid + 0.6*'pin-ooH' + 0.4*O3 @4.30E-13*EXP(1040/TK);
R[AP_32] = 'pin-ooH' ----> pinO2 + OH @ j[COOH_to_HO2];
R[AP_33] = 'pin-ooH' + OH ----> pinO2 + HO2 @1.92E-12*EXP(190/TK);
R[AP_34] = pinO2 + HO2 ----> 'pin-ooH' + OH @2.10E-13*EXP(1320/TK);
R[AP_35] = C8O2 + HO2 ----> 'vol-oxy' @2.10E-13*EXP(1320/TK);
R[AP_36] = oxypinald ----> 0.7*oxypinO2 +1.3*CO + 1.6*HO2 + 0.3*oxyC8O2 + 0.3*XO2 @j[OXYPINALD_to_OXYPINO2];
R[AP_37] = oxypinO2 + NO ---->0.72*oxypinald + 0.8*HO2 + 0.82*NO2 + 0.18*'OH-apNO3' @4.10E-12*EXP(180/TK);
R[AP_38] = oxyC8O2 + NO ----> 0.84*NO2 + 0.711*'vol-oxy' + 0.8*HO2 + 0.16*'OH-apNO3' @4.10E-12*EXP(180/TK);
R[AP_39] = oxypinald + OH ----> 0.8*'oxypin-oo' + 0.1*C2O3 + 0.3*PAR + 0.3*XO2 @9.10E-11;
R[AP_40] = oxypinald + NO3 ----> 0.8*'oxypin-oo' + 0.12*C2O3 + 0.36*XO2 + 0.24*PAR + 1*HO2 + HNO3 @5.40E-14;
R[AP_41] = 'oxypin-oo' + NO ----> NO2 + oxypinO2 @4.10E-12*EXP(180/TK);
R[AP_42] = 'oxypin-oo' + NO2 ----> 'pinald-PAN' @1.02E-19*EXP(5500/TK);
R[AP_43] = 'oxypin-oo' + XO2 ----> oxyC8O2 @3.99E-14;
R[AP_44] = oxypinO2+ HO2 ----> 'pin-ooH' @1.43E-13*EXP(1380/TK);
R[AP_45] = 'oxypin-oo' + HO2 ----> 0.4*oxypinacid + 0.6*'pin-ooH' @4.30E-13*EXP(1040/TK);

SCALAR

RO2 = n['ap-oo']+n['apNO3-oo']+n['pinald-oo']+n['oxypin-oo']+n['predi-oo']+n[pinO2]+n[oxypinO2]+n[P3O2]+n[C8O2]+n[oxyC8O2];

R[AP_46] = pinalic ----> C8O2 + 0.3*XO2 + 2*HO2 @j[pinalic_to_P3O2];
R[AP_49] = pinalic + OH ---->0.71*'predi-oo' + 0.4*XO2 + 0.6*PAR + 0.2*C8O2 @9.10E-11;
R[AP_50] = pinalic + NO3 ----> 0.8*'predi-oo' + 0.6*PAR + 0.15*'stab-oxy' + HNO3 @5.40E-14;
R[AP_51] = 'predi-oo' + NO ----> C8O2 + NO2 + HO2 @4.10E-12*EXP(180/TK);
R[AP_52] = 'predi-oo' + NO2 ----> 'pinald-PAN' @1.01E-19*EXP(5500/TK);
R[AP_53] = 'predi-oo' + HO2 ----> 0.4*diacid + 0.6*'pin-ooH' @4.30E-13*EXP(1040/TK);
R[AP_54] = 'ap-oo' ----> 0.35*pinald + 0.06*FORM + 0.7155*'vol-oxy' + 0.2*HO2 @1.50E-13*EXP(818/TK)*RO2;
R[AP_55] = 'apNO3-oo' ----> 0.175*'OH-apNO3' + 0.7155*'vol-oxy' + 0.075*FORM + 0.175*pinald + 0.075*HO2 @1.50E-13*EXP(416/TK)*RO2;
R[AP_56] = C8O2 ----> 0.885*'vol-oxy' + 0.6*HO2 @1.63E-15*EXP(1961/TK)*RO2;
R[AP_57] = 'pinald-oo' ----> 0.263*pinO2 + 0.1125*pinacid + 0.25*'vol-oxy' + 0.238*pinald + 0.18*'OH-apNO3' + 0.5*CO2 @5.09E-12*EXP(272/TK)*RO2;
R[AP_58] = pinO2 ----> 0.74*pinald + 0.1775*'vol-oxy' + 0.6*HO2 @1.62E-15*EXP(1961/TK)*RO2;
R[AP_59] = 'oxypin-oo' ----> 0.7*oxypinO2 + 0.3*oxypinacid + 0.7*CO2 + 0.6*HO2 @1.62E-15*EXP(1961/TK)*RO2;
R[AP_60] = oxypinO2 ----> 0.74*oxypinald + 0.1775*'vol-oxy' + 0.6*HO2 @3.73E-11*EXP(416/TK)*RO2;
R[AP_61] = 'predi-oo' ----> 0.5*C8O2 + 0.3*pinalic + 0.6*HO2 + 0.6*CO2 @1.70E-11*EXP(417/TK)*RO2;
R[AP_64] = 'OH-apNO3' + OH ----> NO2 + pinald @1.5E-11;
R[AP_65] = 'ap-oo' + XO2 ----> 'vol-oxy' + HO2 @3.99E-14;
R[AP_66] = 'apNO3-oo' + XO2 ----> 'OH-apNO3' + HO2 @3.99E-14;
R[AP_67] = pinO2 + XO2 ----> 0.8*'vol-oxy' + HO2 +0.6*CO2+ 0.18*pinald @3.99E-18;
R[AP_68] = C8O2 + XO2 ----> 0.88*'vol-oxy' + HO2 @3.99E-18;
R[AP_69] = 'pinald-oo' + XO2 ----> pinO2 + HO2 @5.09E-12*EXP(272/TK);
R[AP_71] = pinacid + OH ----> 'pre-tri' + HO2 @5.34E-18*TK^2*EXP(-230/TK);

```
// {Gas Wall Losses}
 R[gwall_64] = diacid ---->                                  @1.00E-08*EXP(2445/TK);
 R[gwall_65] = oxypinacid ---->                              @1.00E-08*EXP(2445/TK);
 R[gwall_66] = pinacid ---->                                 @6.67E-09*EXP(2445/TK);
 R[gwall_67] = oxypinald ---->                               @6.67E-09*EXP(2445/TK);
 R[gwall_68] = pinalic ---->                                 @6.67E-09*EXP(2445/TK);
 R[gwall_69] = pinald ---->                                  @4.167E-09*EXP(2445/TK);
 R[gwall_70] = 'OH-apNO3' ---->                              @1.167E-08*EXP(2445/TK);
 R[gwall_71] = 'pinald-PAN' ---->                            @1.167E-08*EXP(2445/TK);

// {Oligomer Reactions}
 R[olig_72] = part2 + part2 ----> seed1                      @4.74E-15;
 R[olig_73] = part2 + part1 ----> seed1                      @6.77E-16;
 R[olig_74] = part2 + part3 ----> seed1                      @2.03E-15;
 R[olig_75] = part2 + part5 ----> seed1                      @3.39E-16;
 R[olig_76] = part2 + part ----> seed1                       @6.77E-17;

// {Partitioning Reactions}
 R[part_77] = stabcrieg1 + pinald ----> seed1                @1.56E-14;
 R[part_78] = stabcrieg1 + pinacid ----> seed1               @5.30E-13;
 R[part_79] = stabcrieg1 + oxypinald ----> seed1             @1.56E-14;
 R[part_80] = stabcrieg1 + pinalic ----> seed1               @5.30E-13;
 R[part_81] = stabcrieg1 + FORM ----> oxypinald              @1.56E-14;
 R[part_82] = stabcrieg1 + oxypinacid ----> seed1            @5.30E-13;
 R[part_83] = stabcrieg2 + pinald ----> seed1                @1.56E-14;
 R[part_84] = stabcrieg2 + pinacid ----> seed1               @5.30E-13;
 R[part_85] = stabcrieg2 + oxypinald ----> seed1             @1.56E-14;
 R[part_86] = stabcrieg2 + pinalic ----> seed1               @5.30E-13;
 R[part_87] = stabcrieg2 + FORM ----> oxypinald              @1.56E-14;
 R[part_88] = stabcrieg2 + oxypinacid ----> seed1            @5.30E-13;
 R[part_89] = diacid + diacid ----> seed1                    @3.39E-17;
 R[AP_72] = 'pre-tri' ----> part8                            @1.245E-2*EXP(-7070/TK);
 R[AP_73] = 'OH-apN2O6' ----> part9                          @3.737E-2*EXP(-7250/TK);
 R[AP_74] = part8 ----> 'pre-tri'                            @6.21E12*EXP(-11564/TK);
 R[AP_75] = part9 ----> 'OH-apN2O6'                          @6.21E12*EXP(-12039/TK);

SCALAR
Tpart = n[part]+n[part1]+n[part2]+n[part3]+n[part4]+n[part5]+n[part6]+n[part7]+n[part8]+n[part9]+n[seed]+n[seed1];

 R[part_90] = diacid ----> part                              @Tpart*2.198E-4*EXP(-6568/TK);
 R[part_91] = part ----> diacid                              @6.2167E12*EXP(-10142/TK);
```

```
R[part_92] = pinacid ----> part1                          @Tpart*2.66E-5*EXP(-6320/TK);
R[part_93] = part1 ----> pinacid                          @6.2167E12*EXP(-9392/TK);
R[part_94] = pinald ----> part2                           @Tpart*1.889E-6*EXP(-5030/TK);
R[part_95] = part2 ----> pinald                           @6.2167E12*EXP(-8693/TK);
R[part_96] = oxypinald ----> part3                        @Tpart*5.91E-6*EXP(-6160/TK);
R[part_97] = part3 ----> oxypinald                        @6.2167E12*EXP(-8886/TK);
R[part_98] = pinalic  ----> part4                         @Tpart*1.259E-5*EXP(-6230/TK);
R[part_99] = part4 ----> pinalic                          @6.2167E12*EXP(-9095/TK);
R[part_109] = oxypinacid ----> part5                      @Tpart*3.309E-5*EXP(-3030/TK);
R[part_109A] = part5 ----> oxypinacid                     @6.22E12*EXP(-9507/TK);
R[part_110] = 'pinald-PAN' ----> part6                    @Tpart*5.353E-5*EXP(-6209/TK);
R[part_112] = part6 ----> 'pinald-PAN'                    @6.2167E12*EXP(-10200/TK);
R[part_113] = 'OH-apNO3' ----> part7                      @Tpart*2.904E-5*EXP(-5940/TK);
R[part_114] = part7 ----> 'OH-apNO3'                      @6.2167E12*EXP(-8455/TK);

//  {Particle Wall Losses}
R[pwall_115] = part ---->                                 @1.33E-5;
R[pwall_116] = part1 ---->                                @1.33E-5;
R[pwall_117] = part2 ---->                                @1.33E-5;
R[pwall_118] = part3 ---->                                @1.33E-5;
R[pwall_119] = part4 ---->                                @1.33E-5;
R[pwall_120] = part5 ---->                                @1.33E-5;
R[pwall_121] = part6 ---->                                @1.33E-5;
R[pwall_122] = part7 ---->                                @1.33E-5;
R[pwall_123] = part9 ---->                                @1.33E-5;
R[pwall_124] = seed ---->                                 @1.33E-5;
R[pwall_125] = seed1 ---->                                @1.33E-5;
R[pwall_126] = O3 ---->                                   @8.31E-6;
R[pwall_127] = O3 + seed1 ---->                           @2.71E-18;
R[pwall_128] = O3 + part ----> part                       @2.71E-18;
R[pwall_129] = O3 + part1 ----> part1                     @2.71E-18;
R[pwall_130] = O3 + part2 ----> part2                     @2.71E-18;
R[pwall_131] = O3 + part3 ----> part3                     @2.71E-18;
R[pwall_132] = O3 + part4 ----> part4                     @2.71E-18;
R[pwall_133] = O3 + part5 ----> part5                     @2.71E-18;
R[pwall_134] = O3 + part6 ----> part6                     @2.71E-18;
R[pwall_135] = O3 + part7 ----> part7                     @2.71E-18;

#end
```

APPENDIX C: Simulations of 1999 Experiments

All gas-phase plots use the following key:

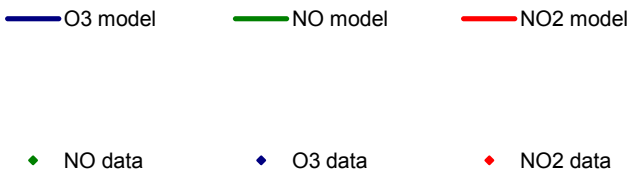

All particle phase plots use the following key:

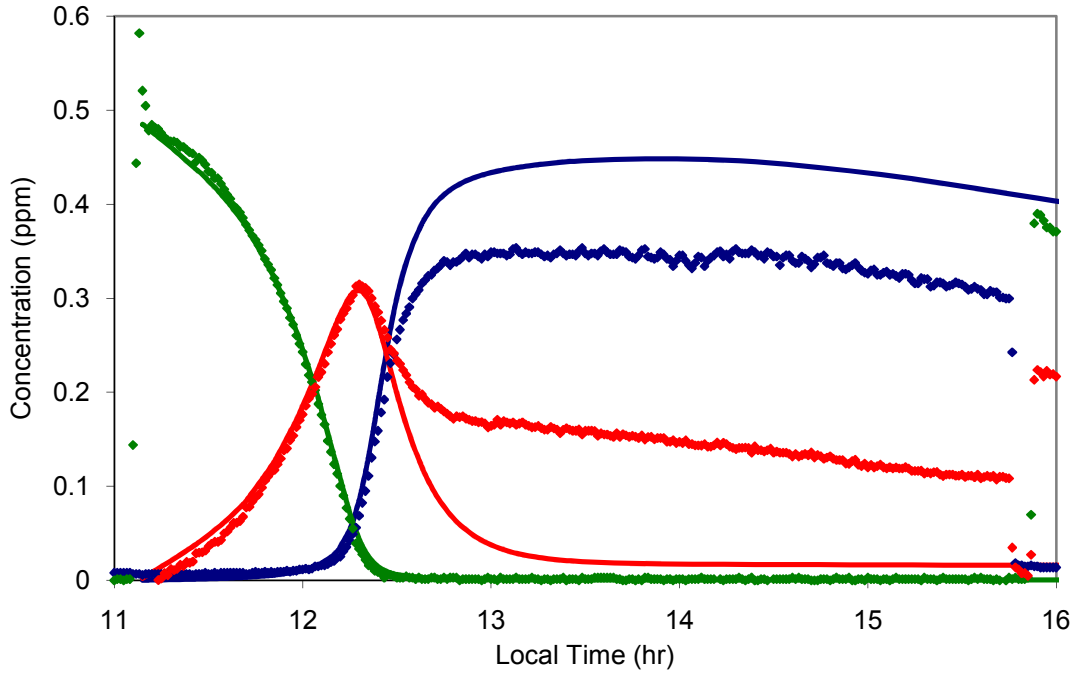

Figure C-1 Model (lines) and data (points) gas-phase results of Experiment 14 (OC3099): 0.95ppmV α-pinene + 0.48ppm NO_x using original UNC mechanism. HC/NO_x ratio: 1.9502

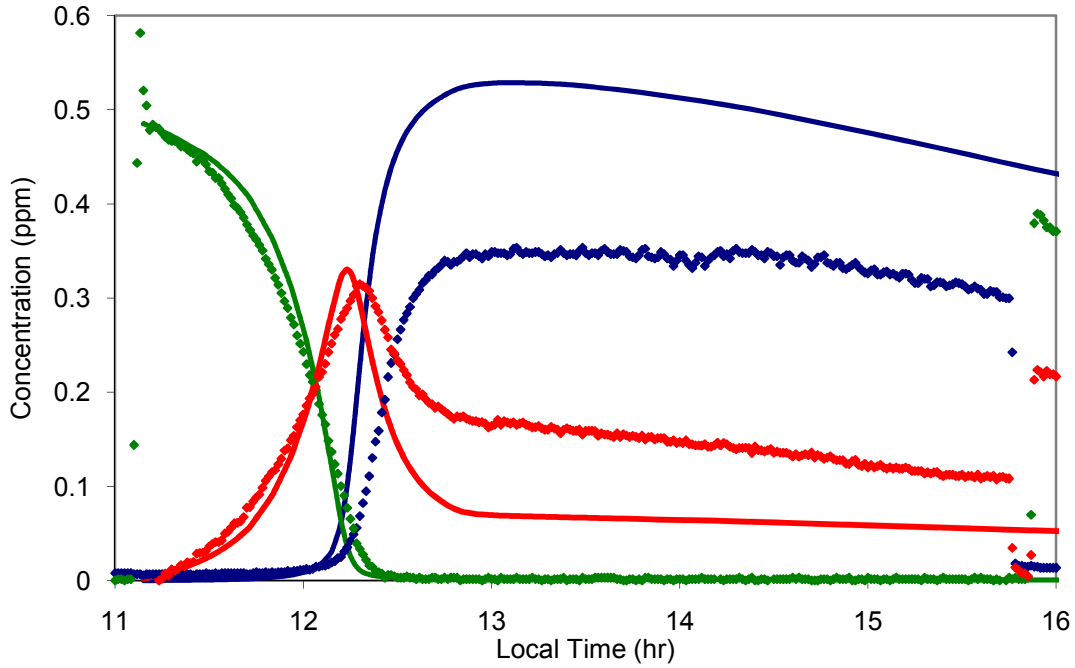

Figure C-2 Model (lines) and data (points) gas-phase results of Experiment 14 (OC3099): 0.95ppmV α-pinene + 0.48ppm NO_x using updated UNC mechanism. HC/NO_x ratio: 1.9502

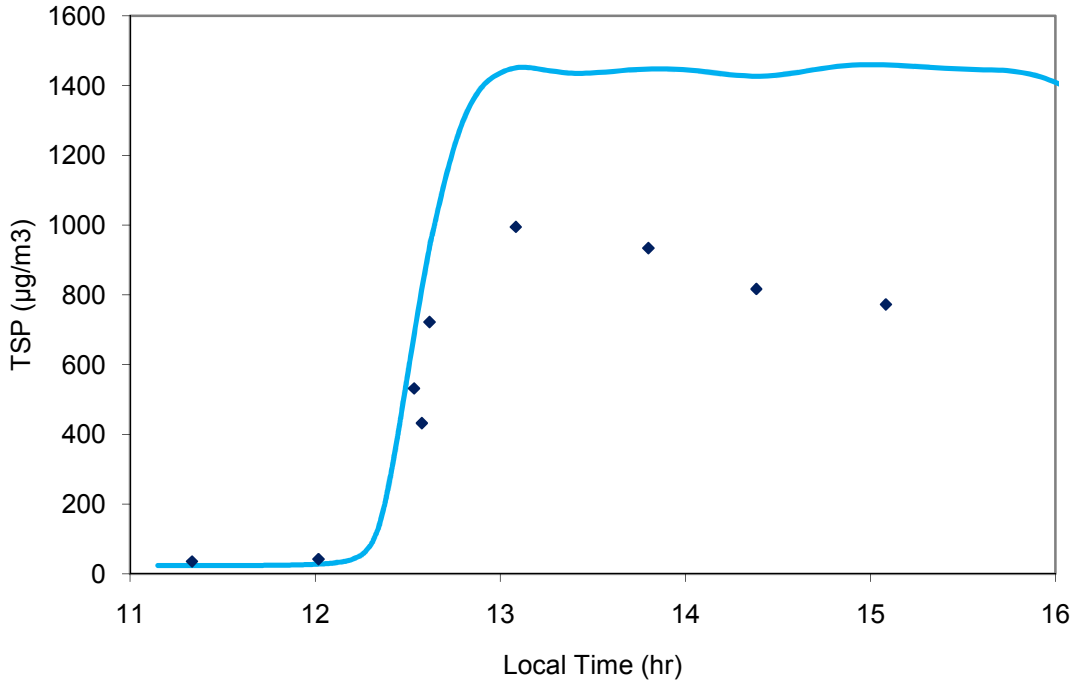

Figure C-3 Model (lines) and data (points) particle-phase results of Experiment 14 (OC3099), 1999: 0.95ppmV α-pinene + 0.48ppm NO_x (HC/NOx ratio of 2.26) using original UNC mechanism. HC/NO_x ratio: 1.9502

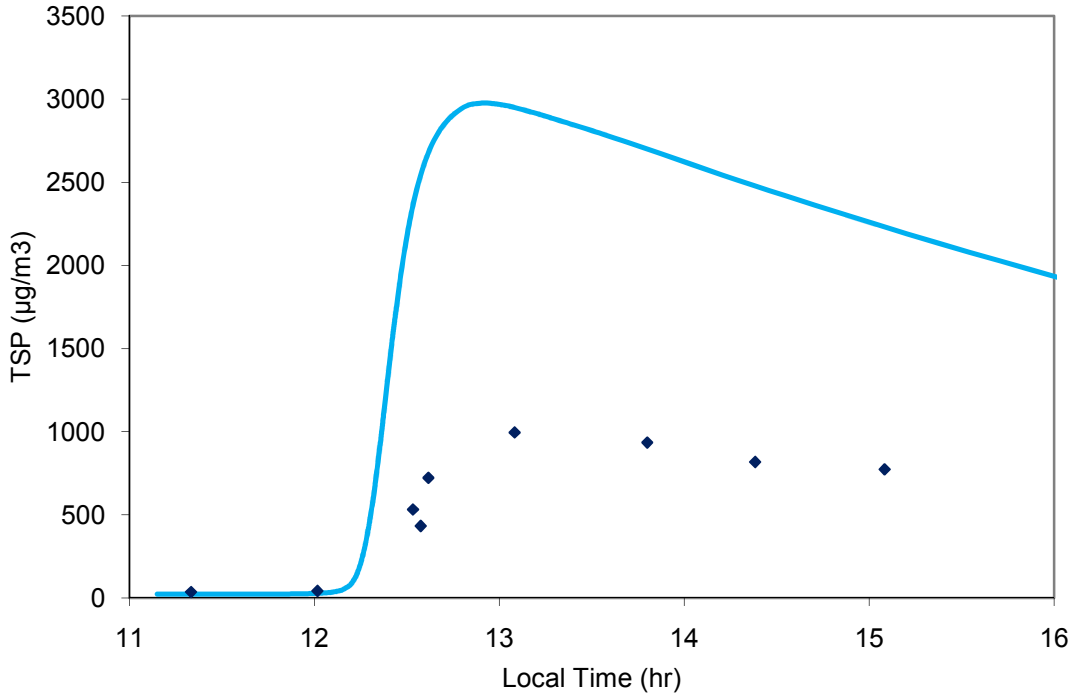

Figure C-4 Model (lines) and data (points) particle-phase results of Experiment 14 (OC3099), 1999: 0.95ppmV α-pinene + 0.48ppm NO_x using updated UNC mechanism. HC/NO_x ratio: 1.9502

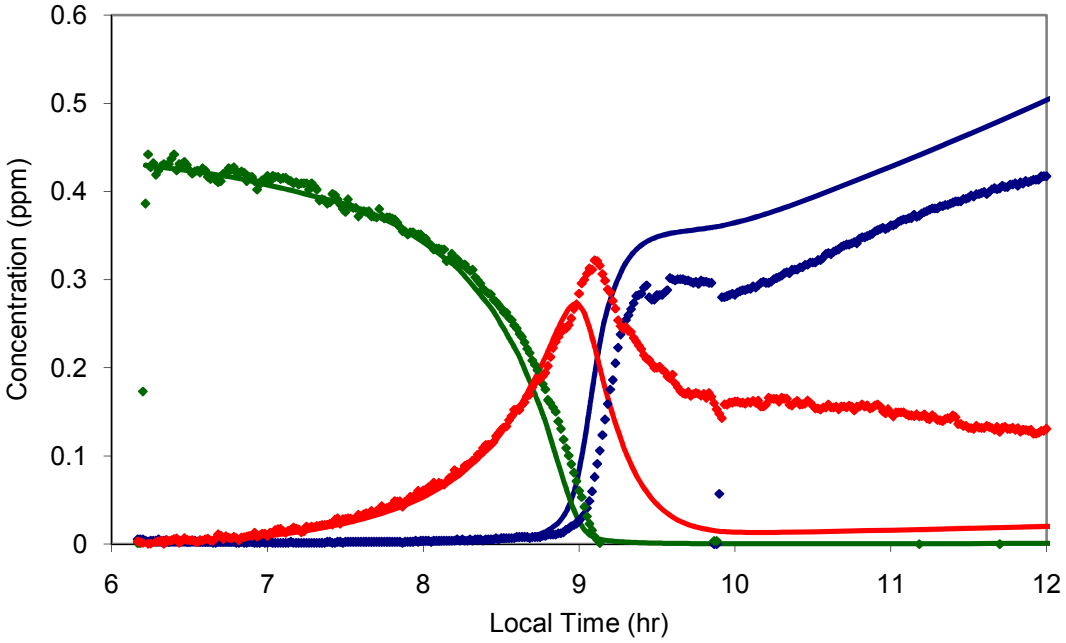

Figure C-5. Model (lines) and data (points) gas-phase results of Experiment 15 (JN0999): 0.98ppmV α-pinene + 0.43ppm NO_x using original UNC mechanism. HC/NO_x ratio: 2.2685

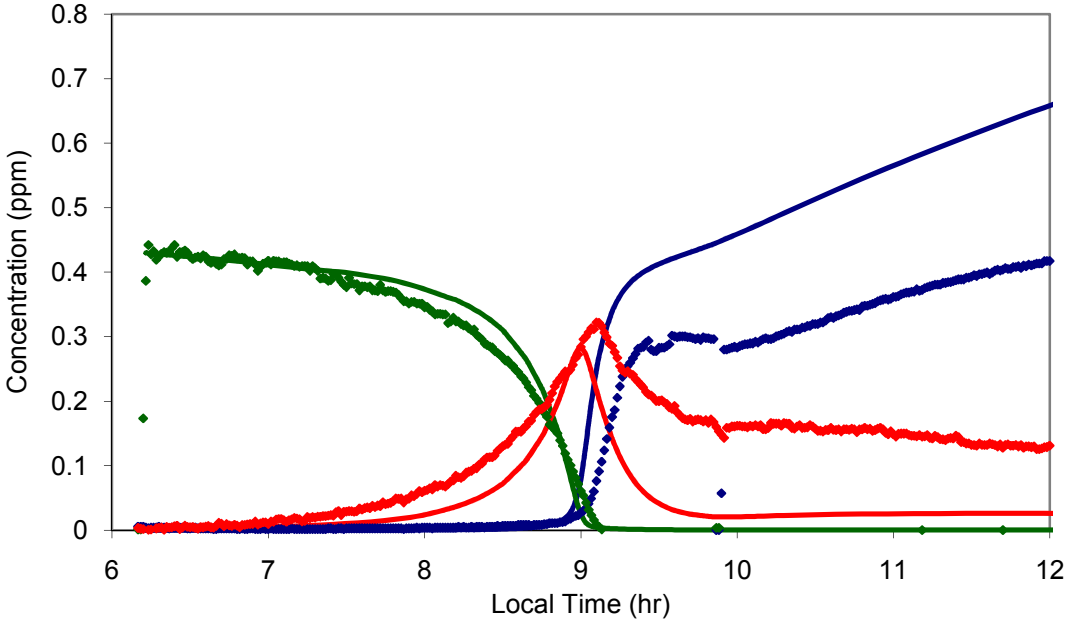

Figure C-6. Model (lines) and data (points) gas-phase results of Experiment 15 (JN0999): 0.98ppmV α-pinene + 0.43ppm NO_x using updated UNC mechanism. HC/NO_x ratio: 2.2685

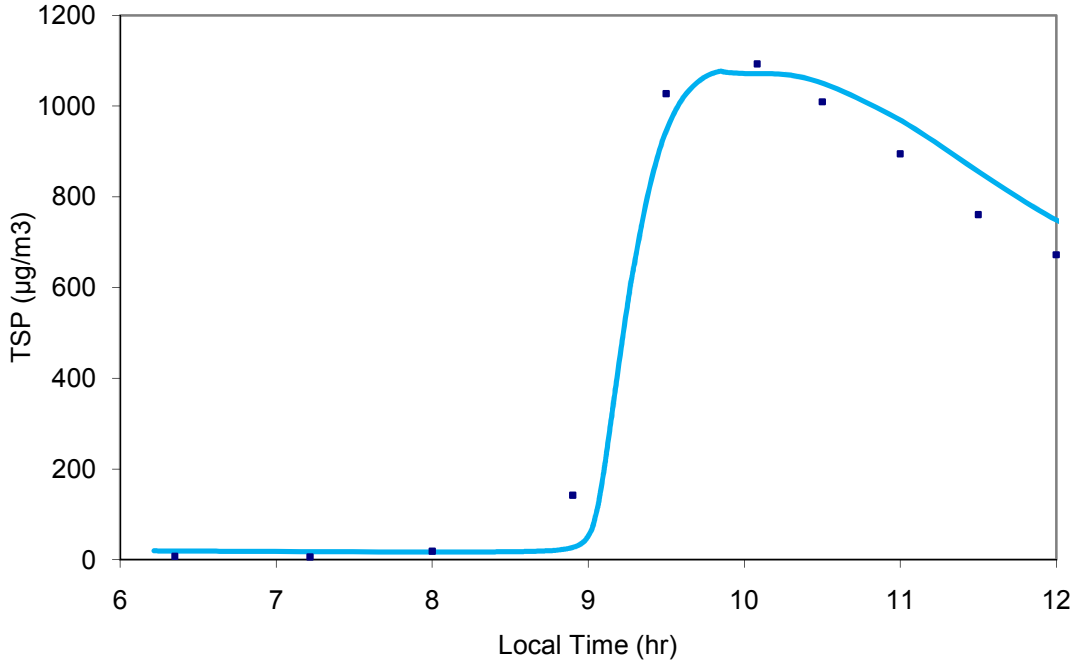

Figure C-7. Model (lines) and data (points) particle-phase results of Experiment 15 (JN0999): 0.98ppmV α-pinene + 0.43ppm NO_x using original UNC mechanism. HC/NO_x ratio: 2.2685

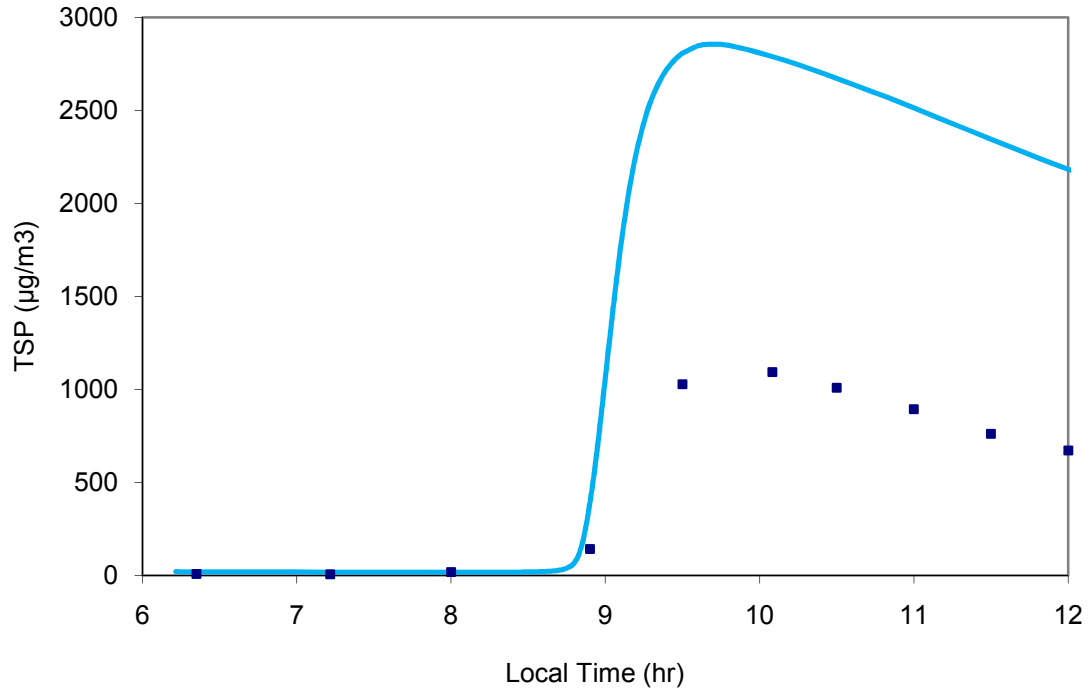

Figure C-8 Model (lines) and data (points) gas-phase results of Experiment 15 (JN0999): 0.98ppmV α-pinene + 0.43ppm NO_x using updated UNC mechanism. HC/NO_x ratio: 2.2685

APPENDIX D: All Gas-Phase and SOA Simulations for 2009, 2010, 2011

All gas-phase plots use the following key:

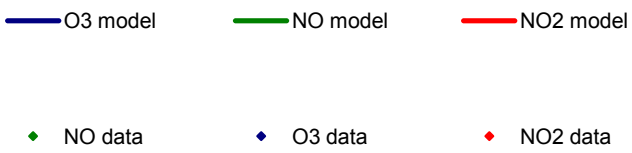

All particle phase plots use the following key:

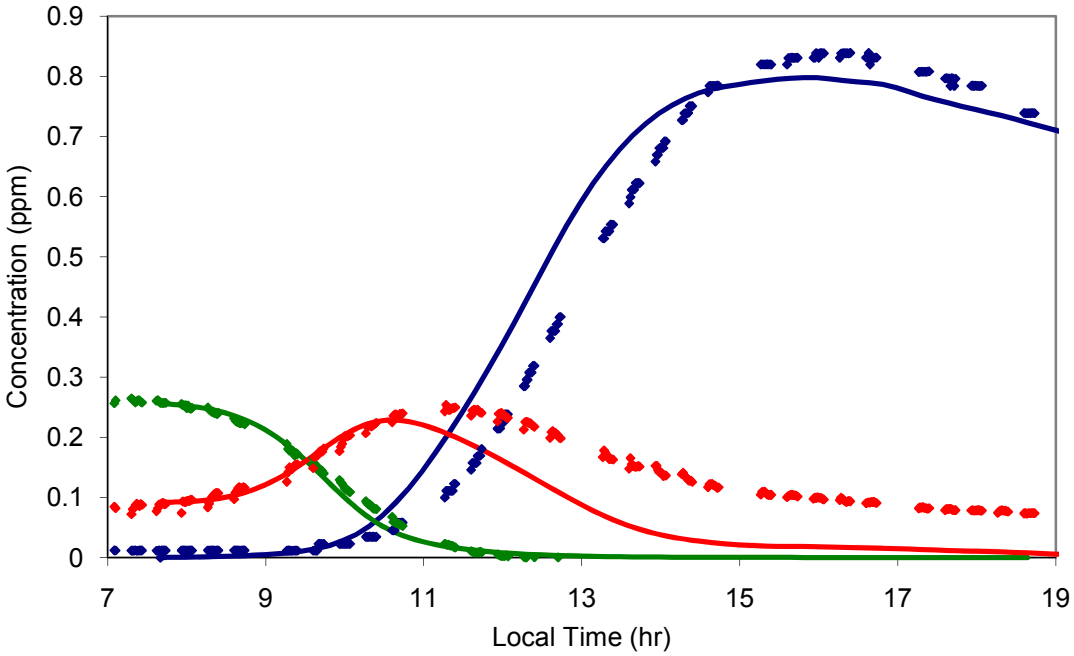

Figure D-1. Model (lines) and data (points) gas-phase results for Experiment 1 (ST0409N): 0.005ppmV α-pinene + 0.2ppm NO_x + 3ppmC HCMix + 0.143ppmV toluene, using updated UNC mechanism. HC/NO_x ratio: 0.0141

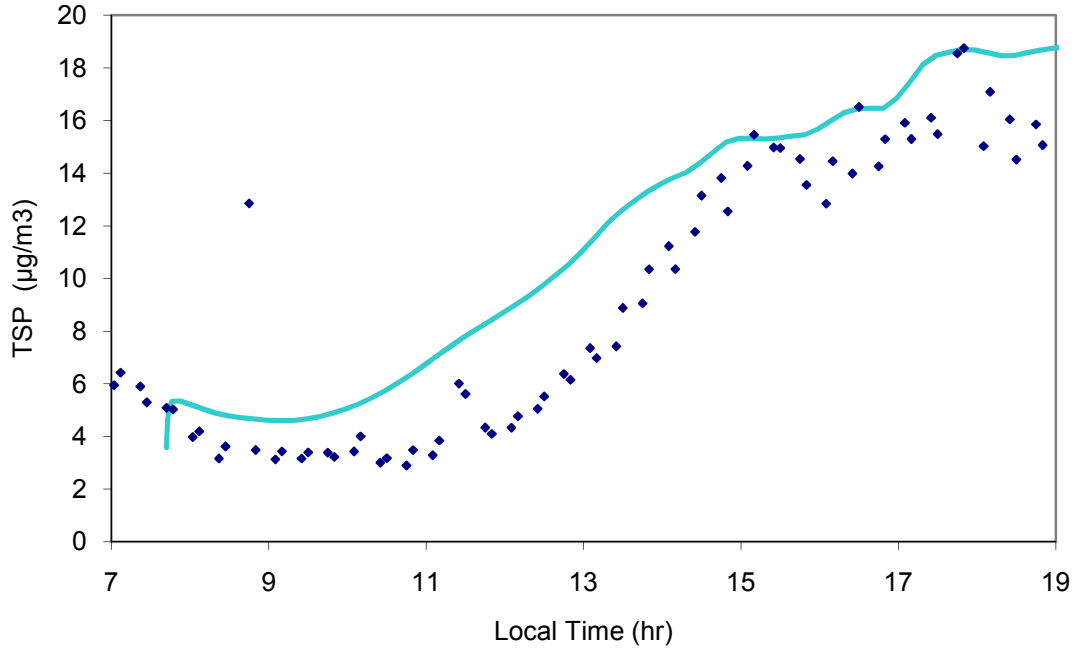

Figure D-2. Model (lines) and data (points) particle-phase results for Experiment 1 (ST0409N): 0.005ppmV α-pinene + 0.2ppm NO_x + 3ppmC HCMix + 0.143ppmV toluene, using updated UNC mechanism. HC/NO_x ratio: 0.0141

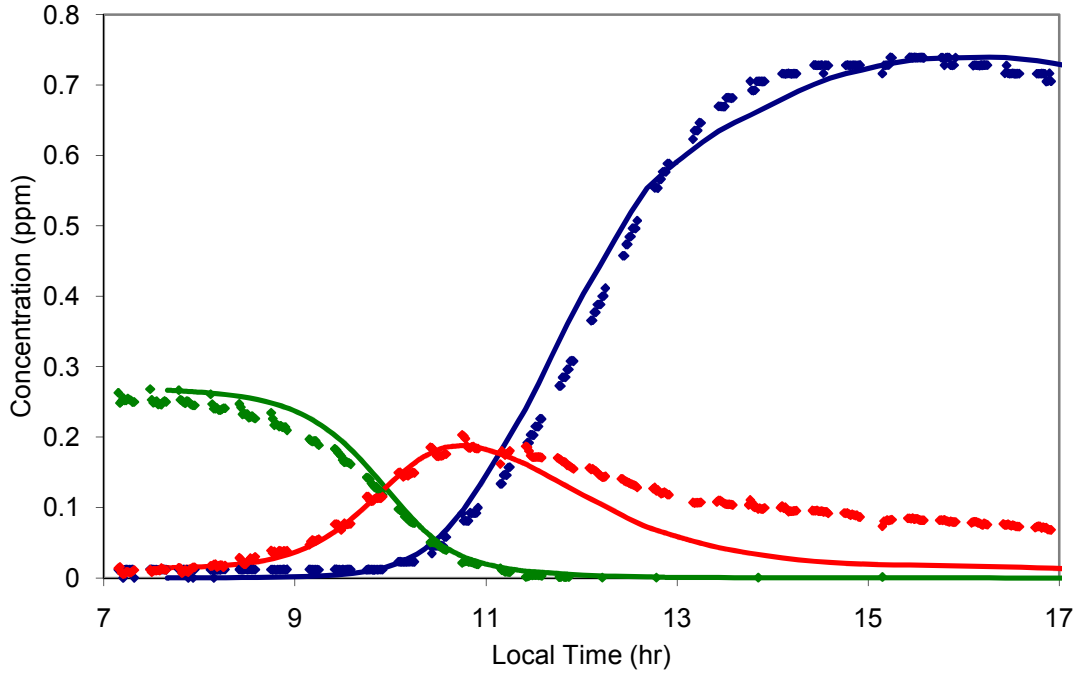

Figure D-3. Model (lines) and data (points) gas-phase results for Experiment 2 (ST0509S): 0.01 ppmV α-pinene + 0.2ppm NO_x + 3ppmC HCMix + 0.143ppmV toluene, using updated UNC mechanism. HC/NO_x ratio: 0.0351

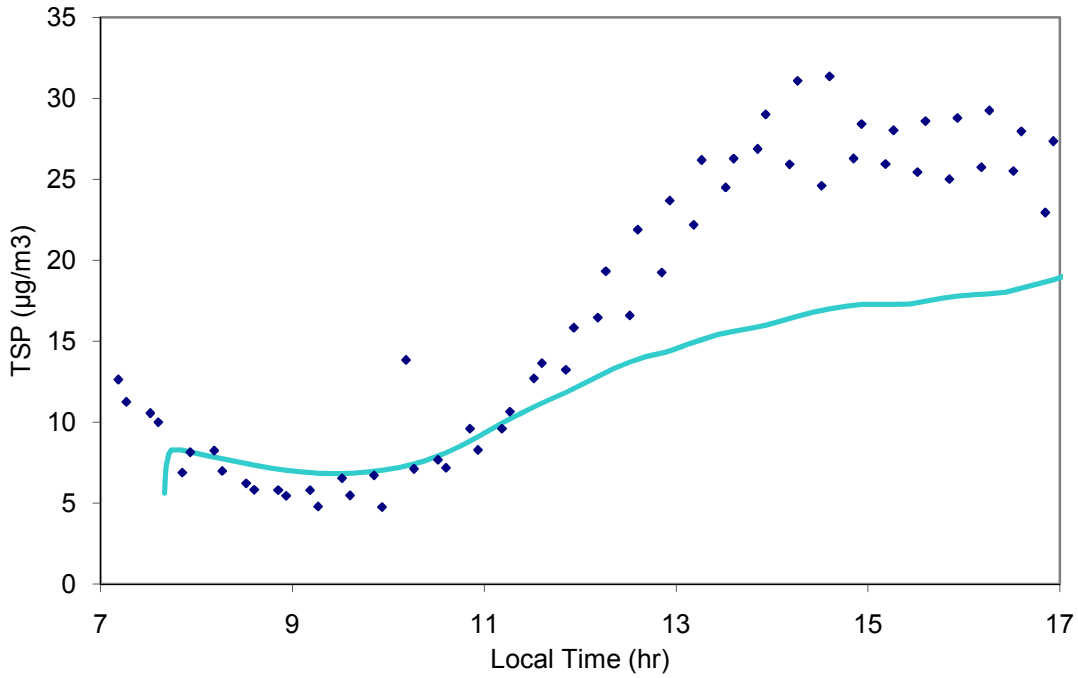

Figure D-4. Model (lines) and data (points) particle-phase results for Experiment 2 (ST0509S): 0.01 ppmV α-pinene + 0.2ppm NO_x + 3ppmC HCMix + 0.143ppmV toluene, using updated UNC mechanism. HC/NO_x ratio: 0.0351

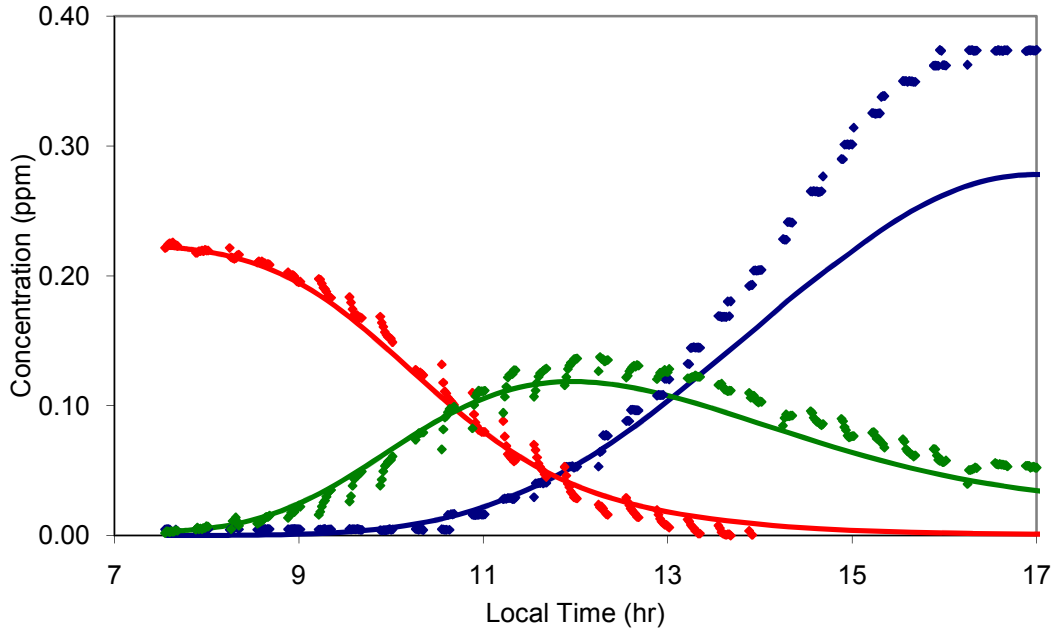

Figure D-5. Model (lines) and data (points) gas-phase results for Experiment 3 (ST1010N): 0.04 ppmV α-pinene + 0.2ppm NO_x + 0.143ppmV toluene, using updated UNC mechanism. HC/NO_x ratio: 0.1792

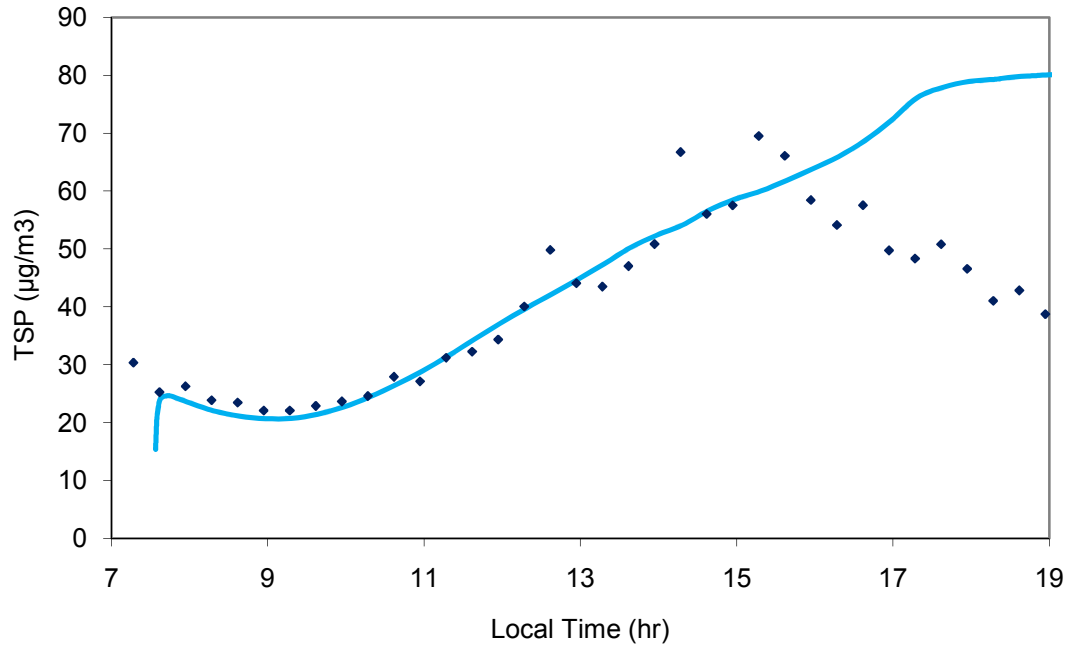

Figure D-6. Model (lines) and data (points) particle-phase results for Experiment 3 (ST1010N): 0.04 ppmV α-pinene + 0.2ppm NO_x + 0.143ppmV toluene, using updated UNC mechanism. HC/NO_x ratio: 0.1792

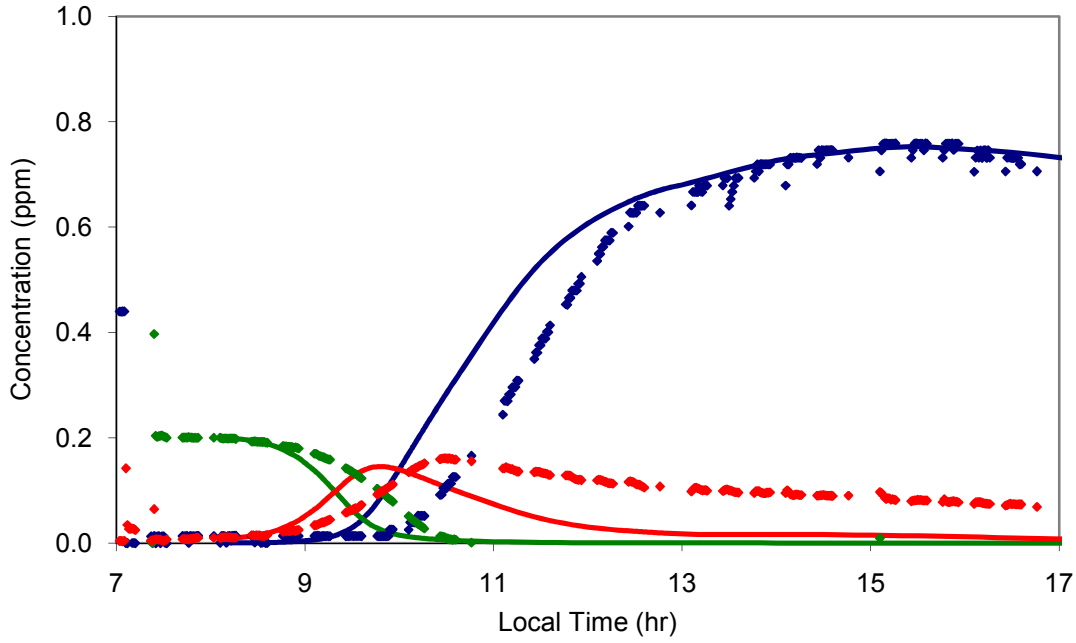

Figure D-7. Model (lines) and data (points) gas-phase results for Experiment 4 (ST1610S): 0.04 ppmV α-pinene + 0.2ppm NO_x + 3ppmC HCMix + 0.143ppmV toluene, using updated UNC mechanism. HC/NO_x ratio: 0.1994

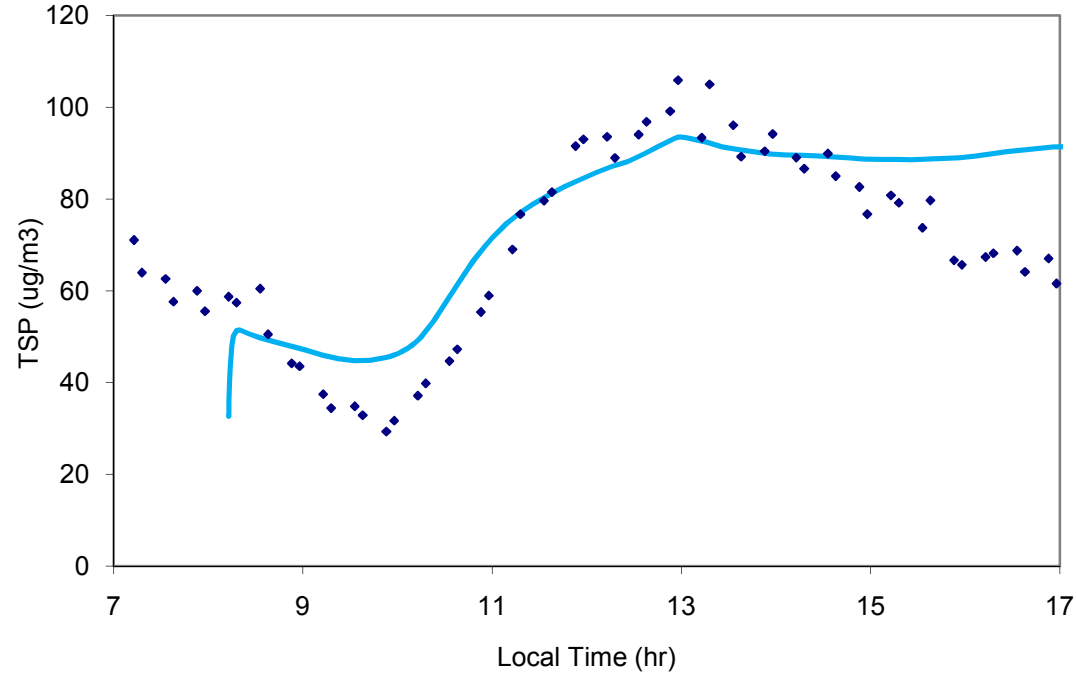

Figure D-8. Model (lines) and data (points) particle-phase results for Experiment 4 (ST1610S): 0.04 ppmV α-pinene + 0.2ppm NO_x + 3ppmC HCMix + 0.143ppmV toluene, using updated UNC mechanism. HC/NO_x ratio: 0.1994

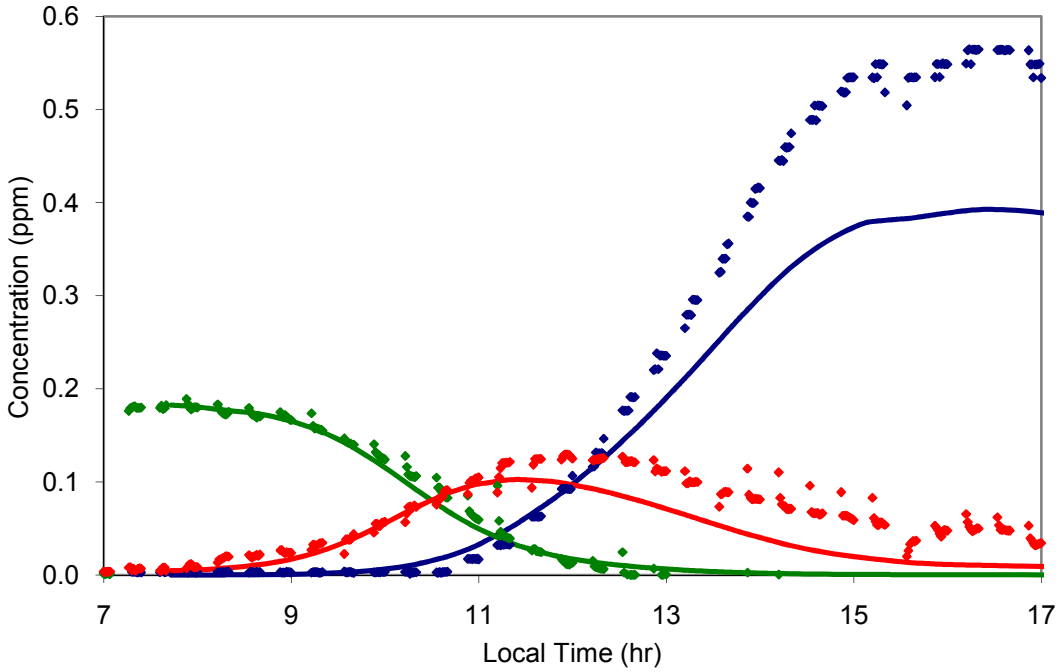

Figure D-9. Model (lines) and data (points) gas-phase results for Experiment 5 (ST0110N): 0.04 ppmV α-pinene + 0.2ppm NO_x + 0.143ppmV toluene, using updated UNC mechanism. HC/NO_x ratio: 0.2168

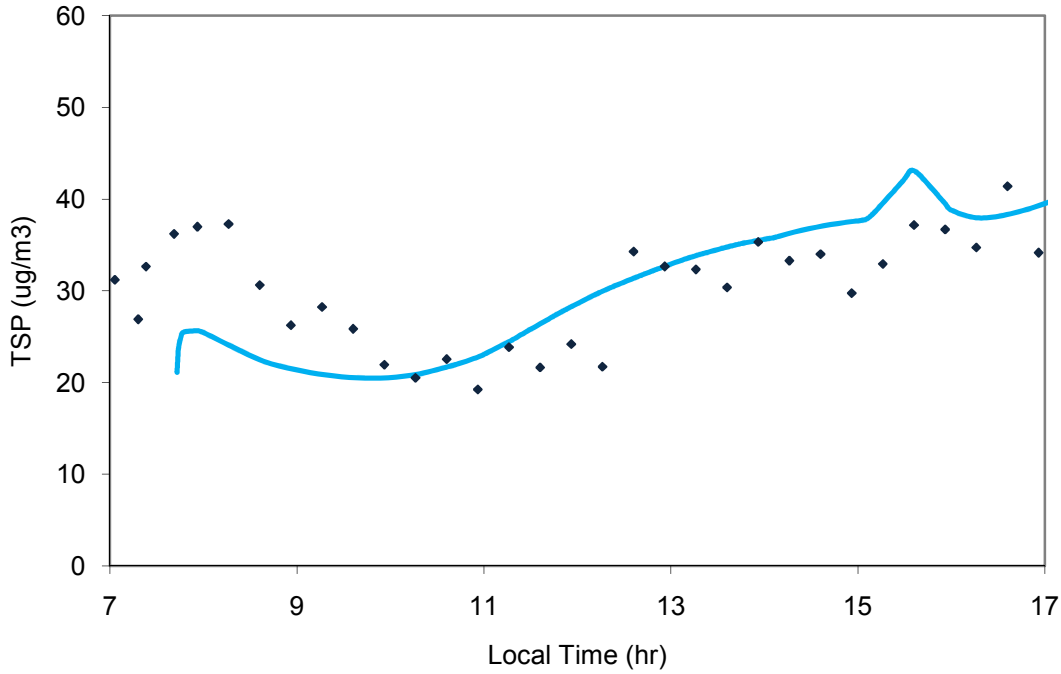

Figure D-10. Model (lines) and data (points) particle-phase results for Experiment 5 (ST0110N): 0.04 ppmV α-pinene + 0.2ppm NO_x + 0.143ppmV toluene, using updated UNC mechanism. HC/NO_x ratio: 0.2168

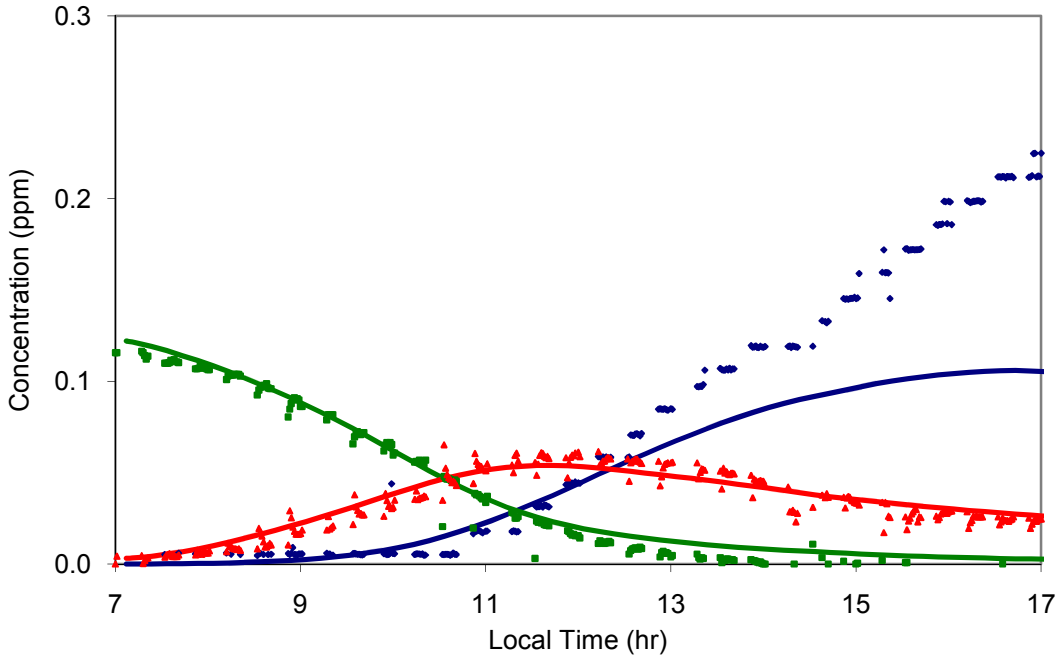

Figure D-11. Model (lines) and data (points) gas-phase results for Experiment 6 (AU0910S): 0.05ppmV α-pinene + 0.1ppm NO_x using updated UNC mechanism. HC/NO_x ratio: 0.4062

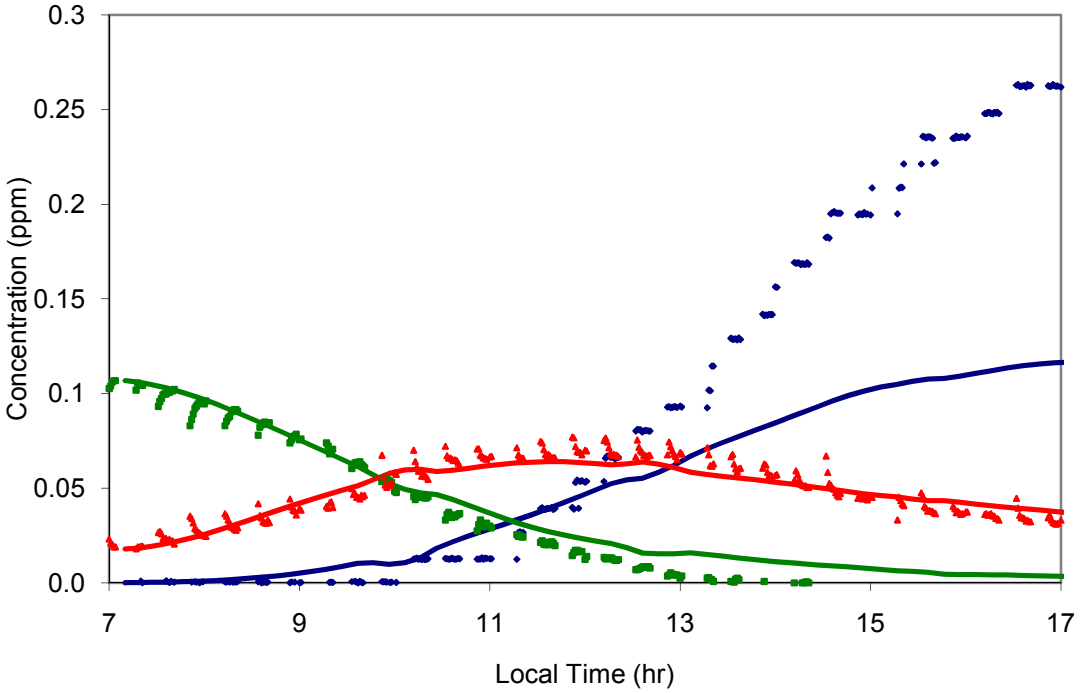

Figure D-12. Model (lines) and data (points) gas-phase results for Experiment 7 (JL3010S): 0.05ppmV α-pinene + 0.1ppm NO_x using updated UNC mechanism. HC/NO_x ratio: 0.4237

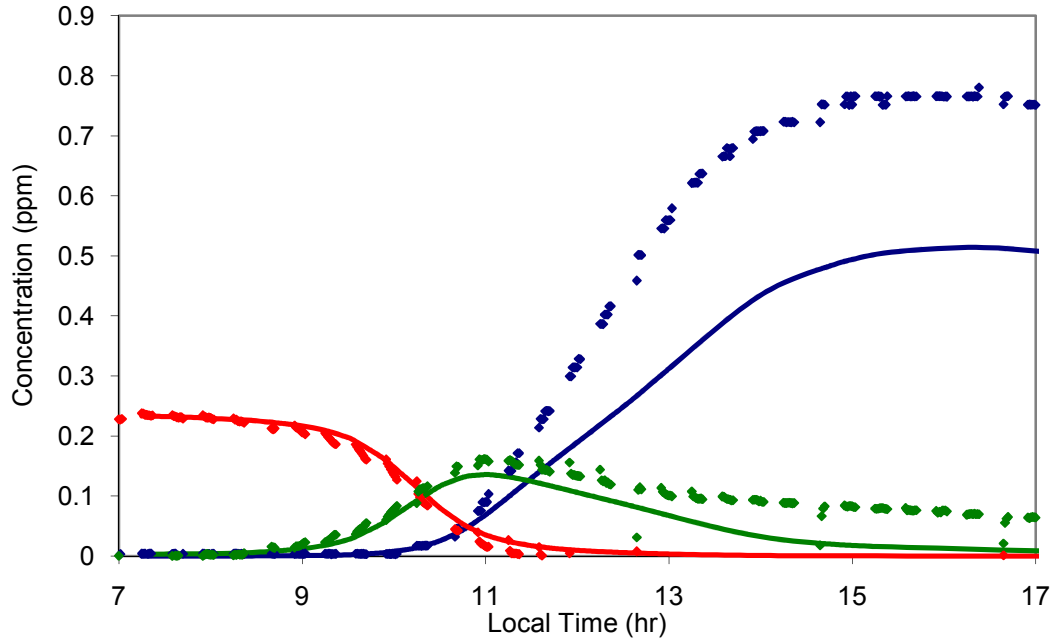

Figure D-13. Model (lines) and data (points) gas-phase results for Experiment 8 (ST1510N): 0.1 ppmV α-pinene + 0.2ppm NO_x + 0.143ppmV toluene, using updated UNC mechanism. HC/NO_x ratio: 0.4288

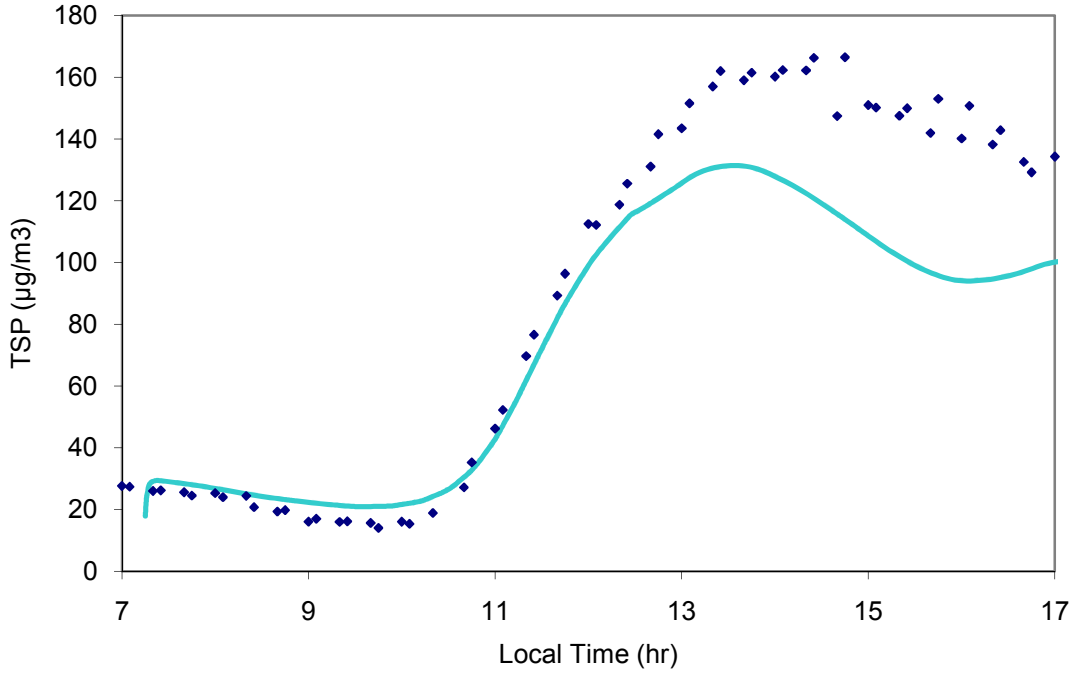

Figure D-14. Model (lines) and data (points) particle-phase results for Experiment 8 (ST1510N): 0.1 ppmV α-pinene + 0.2ppm NO_x + 0.143ppmV toluene, using updated UNC mechanism. HC/NO_x ratio: 0.4288

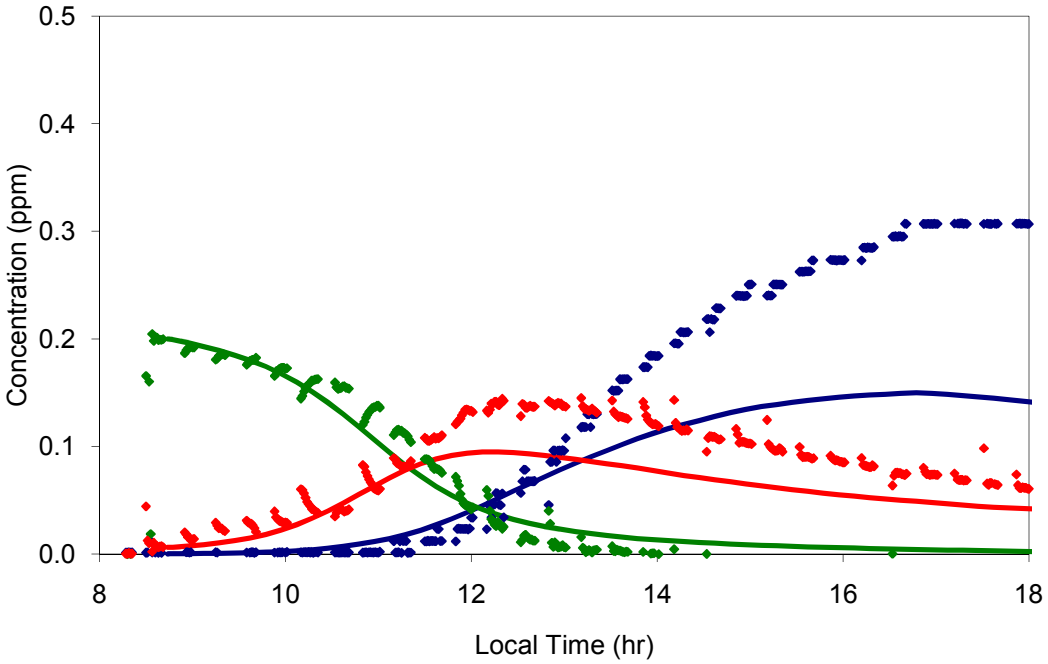

Figure D-15. Model (lines) and data (points) gas-phase results for Experiment 9 (MY1511S): 0.1ppmV α-pinene + 0.2ppm NO_x using updated UNC mechanism. HC/NO_x ratio: 0.4844

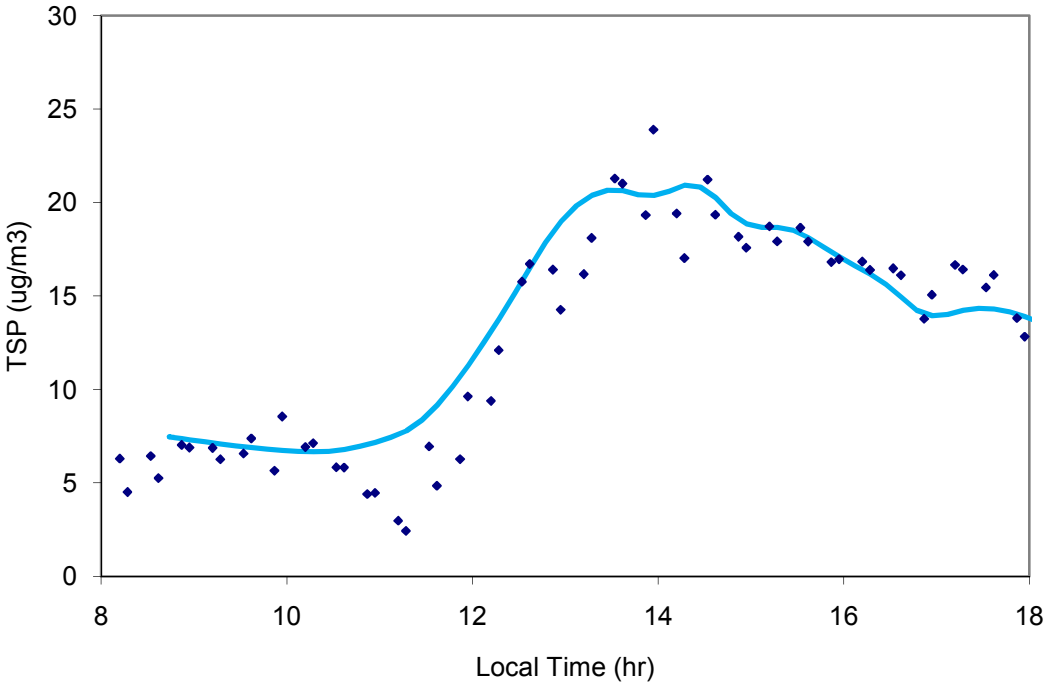

Figure D-16. Model (lines) and data (points) particle-phase results for Experiment 9 (MY1511S): 0.1ppmV α-pinene + 0.2ppm NO_x using updated UNC mechanism. HC/NO_x ratio: 0.4844

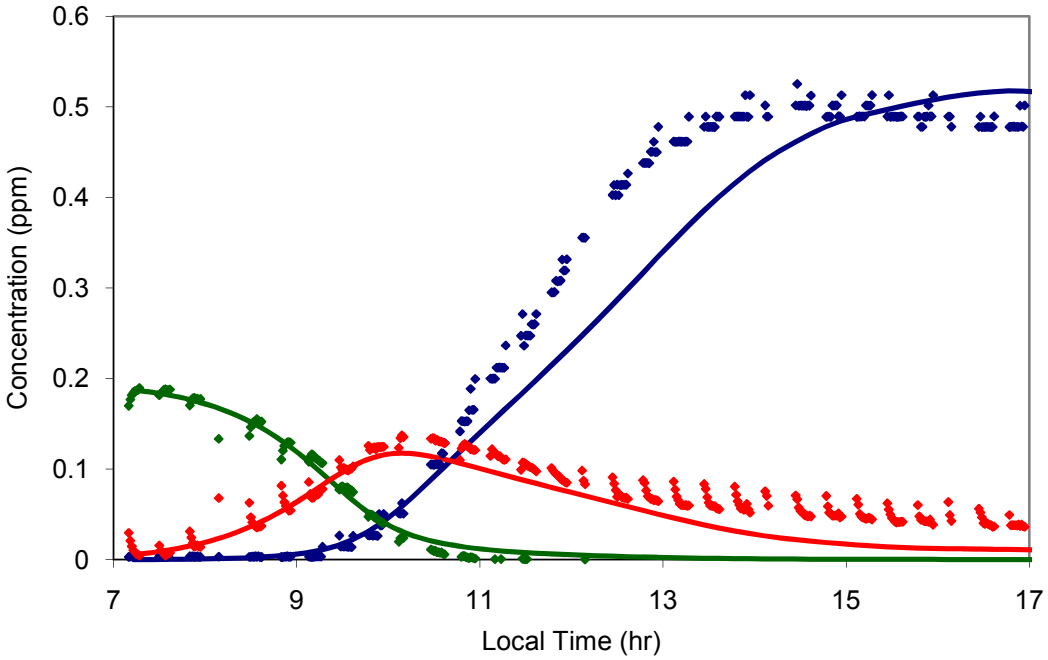

Figure D-17. Model (lines) and data (points) gas-phase results for Experiment 10 (MY2111S): 0.1ppmV α-pinene + 0.2ppm NO_x + 0.1429ppmV toluene using updated UNC mechanism. HC/NO_x ratio: 0.5112

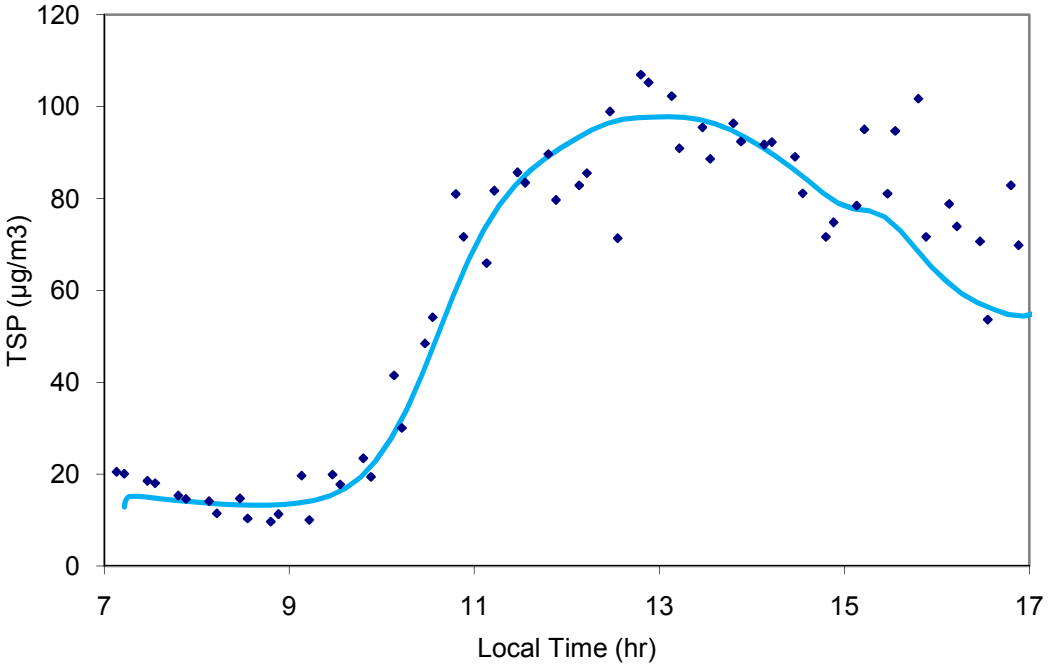

Figure D-18. Model (lines) and data (points) particle-phase results for Experiment 10 (MY2111S): 0.1ppmV α-pinene + 0.2ppm NO_x + 0.1429ppmV toluene using updated UNC mechanism. HC/NO_x ratio: 0.5112

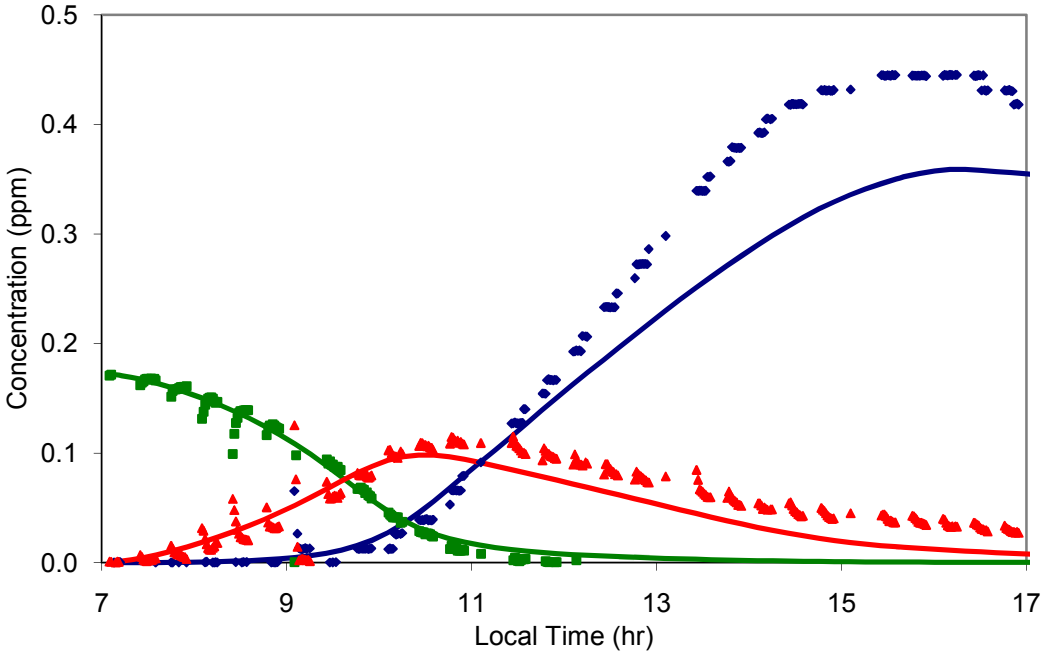

Figure D-19. Model (lines) and data (points) gas-phase results for Experiment 11 (JL2410S): 0.1ppmV α-pinene + 0.2ppm NO_x using updated UNC mechanism. HC/NO_x ratio: 0.5848

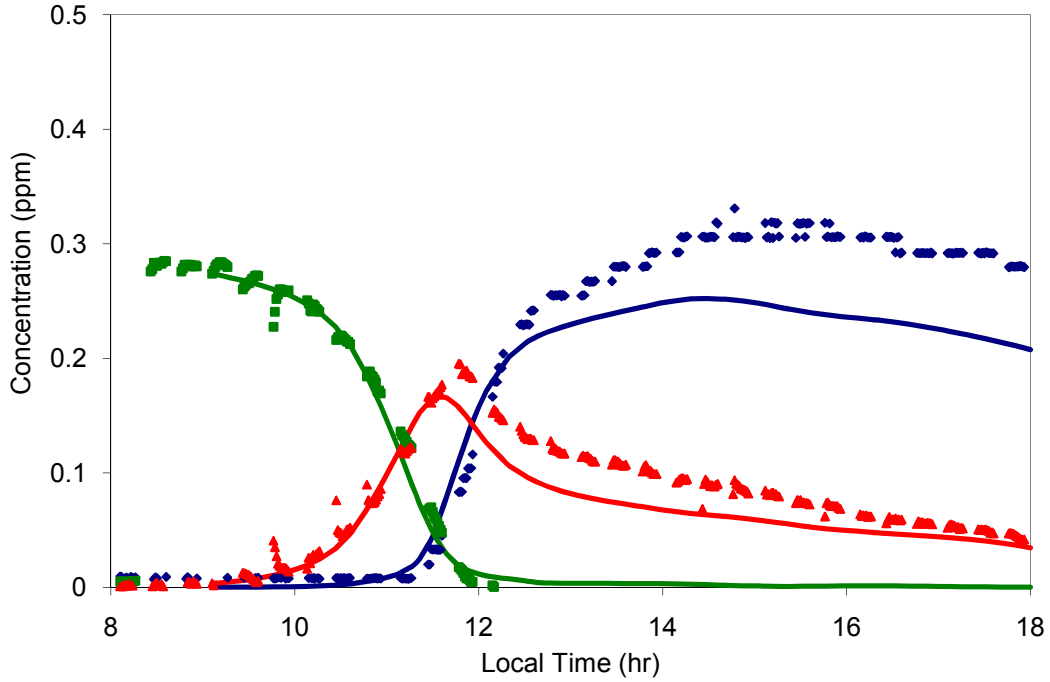

Figure D-20. Model (lines) and data (points) gas-phase results for Experiment 12 (OC1810S): 0.3ppmV α-pinene + 0.3ppm NO_x using updated UNC mechanism. HC/NO_x ratio: 1.0972

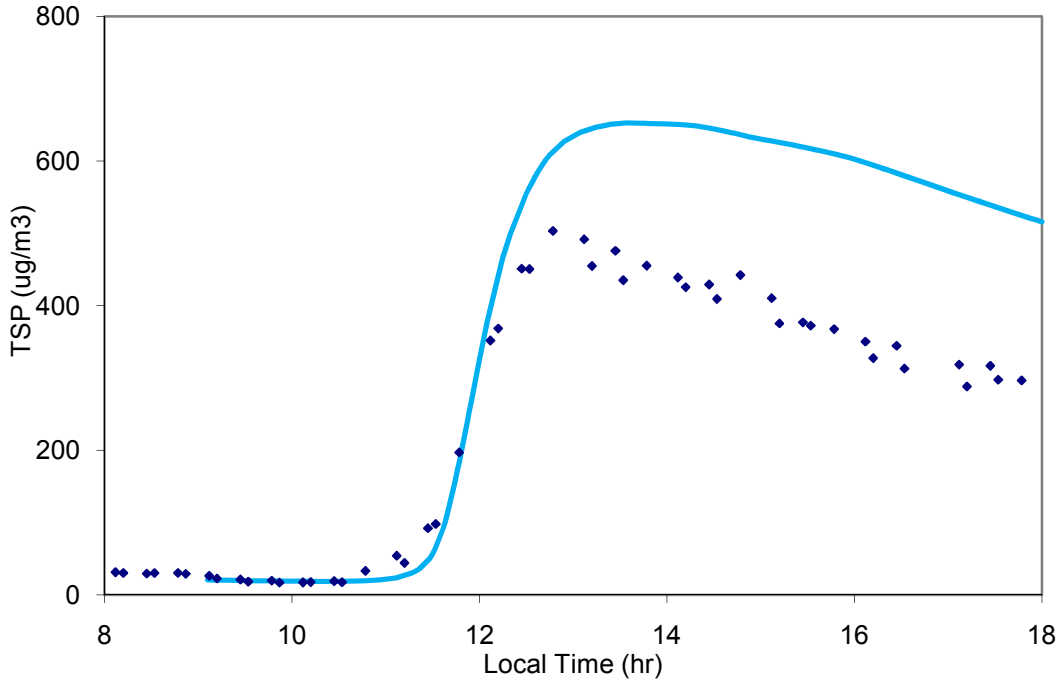

Figure D-21. Model (lines) and data (points) particle-phase results for Experiment 12 (OC1810S): 0.3ppmV α-pinene + 0.3ppm NO_x using updated UNC mechanism. HC/NO_x ratio: 1.0972

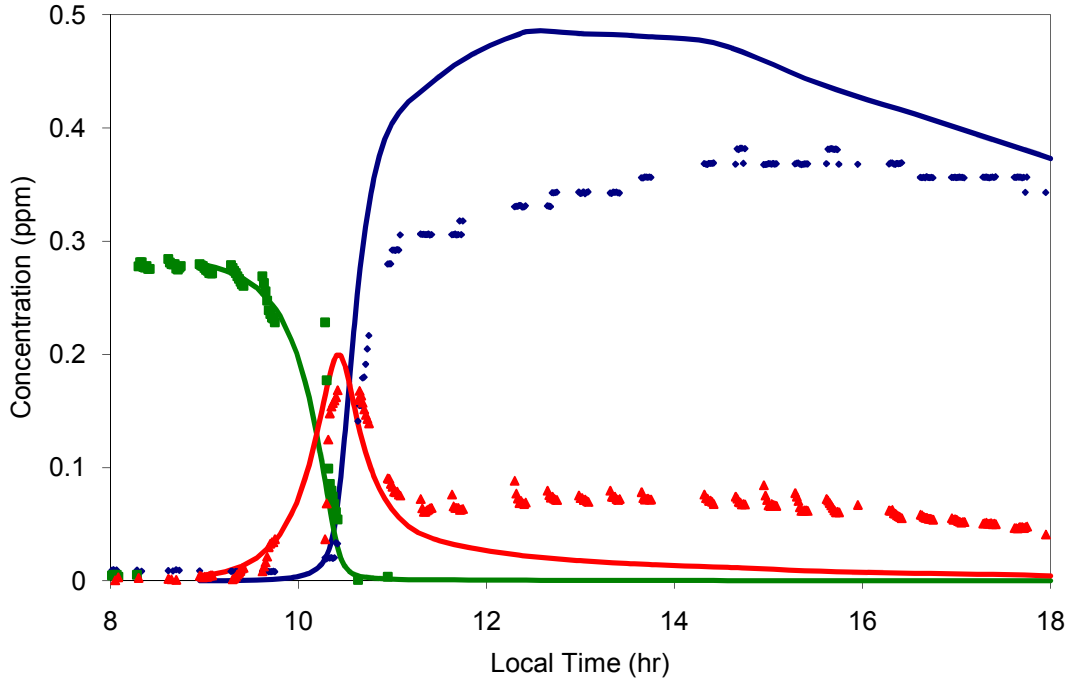

Figure D-22. Model (lines) and data (points) gas-phase results for Experiment 13 (OC1810N): 0.5ppmV α-pinene + 0.3ppm NO_x using updated UNC mechanism. HC/NO_x ratio: 1.7587

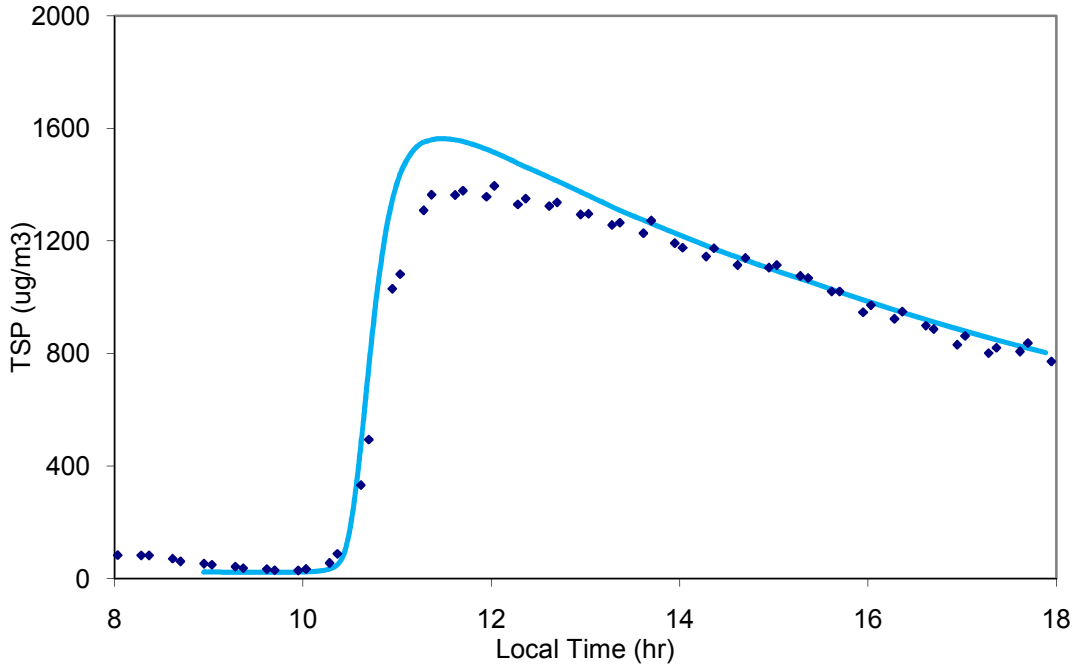

Figure D-23 Model (lines) and data (points) particle-phase results for Experiment 13 (OC1810N): 0.5ppmV α-pinene + 0.3ppm NO_x using updated UNC mechanism. HC/NO_x ratio: 1.7587

REFERENCES

Atkinson, R. (1990). Gas-phase tropospheric chemistry of organic compounds: A review, *Atmos. Environ.*, *24*, 1-41, doi:10:1016/0960-1686(90)90438-S.

Atkinson, R. (1997). Gas-phase tropospheric chemistry of volatile organic compounds: 1. Alkanes and alkenes, *J. Phys. Chem. Ref. Data*, *26*, 215-290, doi:10.1063/1.556012

Blanch, J-S., Llusia, J., Niinemets, U., Noe, S.M., Penuelas, J. (2011). Instantaneous and historical temperature effects on α-pinene emissions in *Pinus halepensis* and *Quercus ilex*, *J. Environ. Biol.*, *32*, 1-6.

Carter, W.P.L. (2009). Development of SAPRC-07 Chemical Mechanism and Updated Ozone Reactivity Scales, Final report to the California Air Resources Board Contract No. 03-318.

Claeys, M., Iinuma, Y., Szmigielski, R., Surratt, J. D., Blockhuys, F., Van Alsenoy, C., Böse, O., Sierau, B., Gómez-González, Y., Vermeylen, R., Van der Veken, P., Shahgholi, M., Chan., A. W. H., Hermann, H., Seinfeld, J., & Maenhaut, W. (2009). Terpenylic acid and related compounds from the oxidation of α-pinene : Implications for new particle formation and growth above forests, *Environ. Sci. Technol.*, *43*, 6976-6982, doi:10:1021/es9007596.

Davis, M. E., Talukdar, R. K., Notte, G., Ellison, G. B., & Burkholder, J. B. (2007). Rate coefficients for the OH + pinonaldehyde ($C_{10}H_{16}O_2$) reaction between 297 and 374 K, *Enriron. Sci. Technol.*, *41*, 3959-3965, doi:10.1021/es070048d

Dlugokencky, E. J., & Howard, C. J. (1989). Studies of nitrate radical reactions with some atmospheric organic compounds at low pressures, *J. Phys. Chem.*, *93*, 1091-1096, doi:10.1021/j100340a015.

Gao, S., Keywood, M., Ng, N. L., Surratt, J., Varutbangkul, V., Bahreini, R., Flagan, R. C., & Seinfeld, J. H. (2004) Low-molecular-weight and oligomeric components in secondary organic aerosol from the ozonolysis of cycloalkenes and α-pinene, *J. Phys. Chem. A*, *108*, 10147-10164, doi: 10.1021/jp047466e.

Gery, M. W., Whitten, G. Z., Killus, J. P., & Dodge, M. C. (1989). A photochemical kinetics mechanism for urban and regional scale computer modeling, *J. Geophys. Res.*, *94*, 12925-12956, doi:10.1029/JD094iD10p12925.

Guenther, A.B., Zimmerman, P.R., Harley, P.C., Monson, R.K., & Fall, R. (1993). Isoprene and monoterpene emission rate variability: Model evaluations and sensitivity analyses, *J. Geophys. Res.*, *98*, 12609-12617, doi:10.1029/93JD00527.

Guenther, A., Hewitt, C.N., Erickson, D., Fall, R., Geron, C., Graedel, T., Harley, P., Klinger, L., Lerdau, M., Mckay, W.A., Pierce, T., Scholes, B., Steinbrecher, R., Tallamraju, R., Taylor, J., & Zimmerman, P. (1995). A global model of natural volatile organic compound emissions, *J Geophys. Res.*, *100*, 8873-8892, doi:10.1029/94JD0950.

Hackney, J.D., Linn, W.S., Mohler, J.G., Pedersen, E.E., Breisacher, P., Russo, A. (1975). Experimental studies on human health effects of air pollutants II: Four-hour exposure to ozone alone and in combination with other pollutant gases, *Arch. Environ. Health*, *30*, 379-384.

Hall IV, W. A., & Johnston, M. V. (2010). Oligomer content of α-pinene secondary organic aerosol, *Aerosol Sci. Tech.*, *45*, 37-45, doi:10.1080/02786826.2010.517580

Hallquist, M., Wängberg, I., & Ljungström, E. (1997). Atmospheric fate of carbonyl oxidation products originating from α-pinene and Δ3-carene: Determination of rate of reaction with OH and NO_3 radicals, UV absorption cross sections, and vapor pressures, *Environ. Sci. Technol.*, *31*, 3166-3172, doi:10.1021/es970151a.

Hallquist, M., Wegner, J.C., Baltensperger, U., Rudich, Y., Simpson, D., Claeys, M., Dommen, J., Donahue, N.M., George, C., Goldstein, A.H., Hamilton, J.F., Herrmann, H., Hoffmann, T., Iinuma, Y., Jang, M., Jenkin, M.E., Jimenez, J.L., Kiendler-Scharr, A., Maenhaut, W., McFiggans, G., Mentel, Th. F., Monod, A., Prevot, A.S.H., Seinfeld, J.H., Surratt, J.D., Szmigielski, R., & Wildt, J. (2009). The formation, properties and impact of secondary organic aerosol: current and emerging issues, *Atmos. Chem. Phys.*, *9*, 5155-5236, doi:10.5194/acp-9-5155-2009.

IUPAC, Subcommittee for gas kinetic data evaluation. 2002.

Jang, M., & Kamens, R. M. (1999) Newly characterized products and composition of secondary aerosols from the reaction of α-pinene with ozone, *Atmos. Environ.*, *33*, 459-474, doi: 10.1016/S1352-2310(98)00222-2.

Jaoui, M., & Kamens, R. M. (2001), Mass balance of gaseous and particulate products analysis from α-pinene/NO_x/air in the presence of natural sunlight, *J. Geophys. Res.*, 106, 12,541–12,558, doi:10.1029/2001JD900005.

Jeffries, H.E., Sexton, K.G., Arnold, J.R., & Kale, T.L. (1989). Validation testing of new mechanisms with outdoor chamber data, Volume 3: Calculation of photochemical reaction photolysis rates in the UNC outdoor chamber. Final Report to the US EPA.

Jeffries, H.E. (1991). PC-Photochemical Kinetics Simulation System (PC-PKSS), Software version 3.0, Department of Environmental Sciences and Engineering, Gillings School of Global Public Health, The University of North Carolina, Chapel Hill, NC 27599.

Jeffries, H.E., Gary, M.W., Kessler, M., Sexton, K.G. (1998). Morphocule reaction mechanism, MORPHO, ALLOMORPHIC simulation software.

Jenkin, M. E., Saunders, S. M., & Pilling, M. J. (1997). The tropospheric degradation of volatile organic compounds: a protocol for mechanism development, *Atmos. Environ.*, *31*, 81-104, doi:10.1016/SI352-2310(96)0105-7

Joback, K. G., & Reid, R. C. (1987). Estimation of pure-component properties from group contributions, *Chem. Eng. Commun.*, *57*, 233-243, doi:10.1080/00986448708960487.

Kamens, R., Jang, M., Chien, C., & Leach, K. (1999). Aerosol formation from the reaction of α-pinene and ozone using a gas-phase kinetics-aerosol partitioning model, *Environ. Sci. Tech.*, *33*, 1430-1430, doi:10:1021/es980725r.

Kamens, R. M., & Jaoui, M., (2001). Modeling aerosol formation from α-pinene + NO_x in the presence of natural sunlight using gas-phase kinetics and gas-particle partitioning theory, *Environ. Sci. Technol.*, *35*, 1394-1405, doi:10.1021/es001626s.

Kamens, R. M., Zhang, H., Chen, E. H., Zhou, Y., Parikh, H. M., Wilson, R. L., Galloway, K. E., & Rosen, E. P. (2011) Secondary organic aerosol formation from toluene in an atmospheric hydrocarbon mixture: Water and particle seed effects, *Atmos. Environ.*, *45*, 2324-2334, doi:10.1016/j.atmosenv/2010.11.007.

Kanakidou, M., Tsigaridis, K., Dentener, F.J., & Crutzen, P.J. (2000). Human-activity-enhanced formation of organic aerosols by biogenic hydrocarbon oxidation, *J. Geophys. Res.*, *105*, 9243-9354, doi:10.1029/1999JD901148.

Kleindienst, T. E., Hudgens, E. E., Smith, D. F., McElroy, F. F., & Bufalini, J. J. (1993). Comparison of chemiluminescence and ultraviolet ozone monitor responses in the presence of humidity and photochemical pollutants, *J. Air Waste Manage.*, *43*(2), 213-222.

Krupnick, A.J., Harrington, W., & Ostro, B. (1990) Ambient ozone and acute health effects: Evidence from daily data, *J. Environ. Econ. Manag.*, *18*, doi:10.1016/0095-0696(90)90048-4.

Leungsakul, S., Jeffries, H.E., & Kamens, R.M. (2005). A kinetic mechanism for predicting secondary aerosol formation from the reactions of d-limonene in the presence of oxides of nitrogen and natural sunlight, *Atmos. Environ.*, *37*, 7063-7082, doi:10.1016/j.atmosenv.2005.08.024.

Lewandowski, M., Jaoui, M., Offenberg, J.H., Kleindienst, T.E., Edney, E.O., Sheesley, R.J., & Schauer, J.J. (2008). Primary and secondary contributions to ambient PM in the Midwestern United States, *Environ. Sci. Tech.*, *42*, 3303-3309, doi:11.1021/es0720412.

Li, Q., Hu, D., Leungsakul, S., & Kamens, R.M. (2007). Large outdoor chamber experiments and computer simulations: (I) Secondary organic aerosol formation from the oxidation of a mixture of d-limonene and α-pinene , *Atmos. Environ.*, *40*, 9341-9352, doi:10.1016/j.atmosenv.2007.09.017.

McDow, S.R., & Huntzicker, J.J. (1990). Vapor adsorption artifact in the sampling of organic aerosol: Face velocity effects, *Atmos. Environ.*, *24*, 2563-2571, doi:10.1016/0960-1686(90)90134-9.

Ng, N. L., Chhabra, P. S., Chan, A. W. H., Surratt, J. D., Kroll, J. H., Kwan, A. J., McCabe, D. C., Wennberg, P. O., Sorooshian, A., Murphy, S. M., Dalleska, N. F., Flagan, R. C., & Seinfeld, J. H. (2007) Effect of NO_x level on secondary organic aerosol (SOA) formation from the photooxidation of terpenes, *Atmos. Chem. Phys.*, *7*, 5159-5174, doi: 10.5194/acp-7-5159-2007.

Pope III, C.A., Burnett, R.T., Thun, M.J., Calle, E.E., Krewski, D., Ito, K., & Thurston, G.D. (2002). Lung cancer, cardiopulmonary mortality, and long-term exposure to fine particle air pollution, *J. Am. Med. Assoc.*, *287*, 1132-1141, doi:10.1001/jama.287.9.1132

Sander, S.P., Ravishankara, A.R., Golden, D.M., Kolb, C.E., Kurylo, M.J., Molina, M.J., Moortgat, G.K., Finlayson-Pitts, B.J., Wine, P.H., & Huie, R.E. (2006). Chemical kinetics and photochemical data for use in atmospheric studies, Evaluation number 15. *JPL Publication,* 06-2.

Saunders, S.M., Jenkin, M.E., Derwent, R.G., & Pilling, M.J. (2003). Protocol for the development of the Master Chemical Mechanism, MCM v3 (Part A): tropospheric degradation of non-aromatic volatile organic compounds, *Atmos. Chem. Phys.*, *3*, 161-180, doi:10.5194/acp-3-161-2003.

Solomon, S., Qin, D., Manning, M., Chen, Z., Marquis, M., Averyt, K., Tignor, M. M.B., Miller, Jr., H.L. (2007). Climate change 2007: The physical science basis, Contribution of Working Group I to the Fourth Assessment Report of the Intergovernmental Panel on Climate Change, Cambridge University Press, Cambridge, UK.

Spittler, M., Barnes, I., Bejan, I., Brockmann, K. J., Benter, Th., & Wirtz, K. (2006). Reactions of NO_3 radicals with limonene and α-pinene : Product and SOA formation, *Atmos. Enriron.*, *40*, S116-S127, doi:10.1016/j.atmosenv.2005.09.093.

Surratt, J. D., Kroll, J. H., Kleindienst, T. K., Edney, E. O., Claeys, M., Sorooshian, A., Ng, N. L., Offenberg, J. H., Lewandowski, M., Jaoui, M., Flagan, R. C., & Seinfeld, J. H. (2007). Evidence for organosulfates in secondary organic aerosol, *Environ. Sci. Tech*, *41*, 517-527, doi: 10.1021/es062081q.

Surratt, J. D., Gómez-González, Y., Chan, A. W. H., Vermeylen, R., Shahgholi, M., Kleindienst, T. E., Edney, E. O., Offenberg, J. H., Lewandowski, M., Jaoui, M., Maenhaut, W., Claeys, M., Flagan, R. C., & Seinfeld, J. H. (2008). Organosulfate formation from biogenic secondary organic aerosol, *J. Phys. Chem. A*, *112*, 8345-8378, doi: 10.1021/jp80231p.

Szmigielski, R., Surratt, J. D., Gómez-González, Y., Van der Veken, P., Kourtchev, I., Vermeylen, R., Blockhuys, F., Jaoui, M., Kleindienst, T. E., Lewandowski, M., Offenberg, J. H., Edney, E. O., Seinfeld, J. H., Maenhaut, W., & Claeys, M. (2007). 3-methyl-1,2,3-butanetricarboxylic acid: An atmospheric tracer for terpene secondary organic aerosol, *Geophys. Res. Lett.*, *34*, L24311, doi:10.1029/2007GL031338.

Tillmann, R., Hallquist, M., Jonsson, Å. M., Keindler-Scharr, A., Saathoff, H., Iinuma, Y., & Mentel, Th. F. (2010). Influence of relative humidity and temperature on the production of pinonaldehyde and OH radicals from the ozonolysis of α-pinene, *Atmos. Chem. Phys.*, *10*, 7053-7072, doi:10.5149/acp-10-7057-2010.

Tolocka, M. P., Jang, M., Ginter, J. M., Cox, F. J., Kamens, R. M., & Johnston, M. V. (2004) Formation of oligomers in secondary organic aerosol, *Environ. Sci. Tech.*, *38*, 1428-1434, doi: 10.1021/es035030r.

Tsigaridis, K., & Kanakidou, M. (2003) Global modeling of secondary organic aerosol in the troposphere: a sensitivity analysis, *Atmos. Chem. Phys.*, *3*, 1849-1869, doi:10.5194/acp-3-1849-2003.

Yarwood, G., Rao, S., Yocke, M., & Whitten, G. Z. (2005). Updates to the Carbon Bond chemical mechanism: CB05, Final Report to the US EPA, RT-0400675.

Yasmeen, F., Vermeylen, R., Szmigielski, R., Iinuma, Y., Böge, O., Herrmann, H., Maenhaut, W., & Claeys, M. (2010). Terpenylic acid and related compounds: precursors for dimers in secondary organic aerosol from the ozonolysis of α- and β-pinene, *Atmos. Chem. Phys.*, *10*, 9383-9392, doi:10.5194/acp-10-9383-2010.

Yu, J., Flagan, R. C., & Seinfeld, J. H. (1998). Identification of products containing –COOH, -OH, and –CO in atmospheric oxidation of hydrocarbons, *Environ. Sci. Tech.*, *32*, 2357-2370, doi: 10.1021/es980129x.

Zhang, H., Rattanavaraha, W., Zhou, Y., Bapat, J., Rose, E. P., Sexton, K. G., & Kamens, R. M. (2011). A new gas-phase condensed mechanism of isoprene-NO_x photooxidation, *Atmos. Environ.*, doi:10.1016/j.atmosenv.2011.04.011.

Zhang, Y. Y., Müller, L., Winterhalter, R., Moortgat, G. K., Hoffmann, T., & Pöschl, U. (2010). Seasonal cycle and temperature dependence of pinene oxidation products, dicarboxylic acids and nitrophenols in fine and coarse air particulate matter, *Atmos. Chem. Phys*., 10, 7859-7873, doi:10.5194/acp-10-7859-2010.